Postfach 10 11 61
69451 Weinheim
Germany
Courier services:
Boschstraße 12
69469 Weinheim
Germany
Tel.: (+49) 6201 606 235 / 432
Fax: (+49) 6201 606 500
E-mail: advmat@wiley-vch.de

Dear Author,

Please correct your galley proofs carefully and return them no more than three days after the page proofs have been received.

If you have not used the PXE system before, please view the Tutorial before checking your proofs: http://wileypxe.aptaracorp.com/pxewileyvch/UserDocument/UserGuide/WileyPXE5_AuthorInstructions.pdf

Please note any queries that require your attention. These are indicated with red Qs in the pdf or highlighted as yellow queries in the "Edit" window.

Please pay particular close attention to the following, as no further corrections can be made once the article is published online:

- **Names** of all authors present and spelled correctly
- **Titles** of authors are correct (Prof. or Dr. only: please note, Prof. Dr. is not used in the journals)
- **Addresses of all authors** and **e-mail address of the corresponding author** are correct and up-to-date
- **Funding bodies** have been included and grant numbers are accurate
- The **Title** of the article is OK
- All **figures** are correctly included
- **Equations** are typeset correctly

Note that figure resolution in the PXE system is deliberately lower to reduce loading times. This will be optimized before the article is published online.

Please send any additional information, such as figures or other display items, to advmat@wiley-vch.de, and please also indicate this clearly in the PXE "Edit" window by inserting a comment using the query tool.

Reprints may be ordered by filling out the accompanying form.
Return the reprint order form by e-mail with the corrected proofs, to Wiley- VCH: **advmat@wiley-vch.de**

Please limit corrections to errors already in the text. Costs incurred for any further changes will be charged to the author, unless such changes have been agreed upon by the editor.

The editors reserve the right to publish your article without your corrections if the proofs do not arrive in time. Note that the author is liable for damages arising from incorrect statements, including misprints.

ADVANCED MATERIALS

Reprint Order Form 2017
- please return with your proofs -

Editorial Office:

Wiley-VCH Verlag, Boschstrasse 12
69469 Weinheim, Germany

Tel.: (+49) 6201 606 235
Fax: (+49) 6201 606 500

E-mail: advmat@wiley-vch.de
http://www.advmat.de

Manuscript No. _____

Please send me and bill me for

☐ no. of **reprints** via ☐ airmail (+ 25 Euro) ☐ surface mail

☐ no. of **copies of this issue** (1 copy: 25 Euro) via ☐ airmail (+ 25 Euro) ☐ surface mail

☐ **high-resolution PDF file** (330 Euro).
My e-mail address:

_____

Please note: It is not permitted to present the PDF file on the internet or on company homepages

★**Special Offer**★ If you order 200 or more reprints you will get a PDF file for half price.

Information regarding VAT
Please note that from German sales tax point of view, the charge for **Reprints, Issues or Posters** is considered as **"supply of goods"** and therefore, in general, such delivery is a subject to German sales tax. However, this regulation has no impact on customers located outside of the European Union. Deliveries to customers outside the Community are automatically tax-exempt. Deliveries within the Community to institutional customers outside of Germany are exempted from the German tax (VAT) only if the customer provides the supplier with his/her VAT number. The VAT number (value added tax identification number) is a tax registration number used in the countries of the European Union to identify corporate entities doing business there. It starts with a country code (e.g. FR for France, GB for Great Britain) and follows by numbers.

Mail reprints /cover posters / copies of the issue to:

_____
_____
_____
_____
_____

Invoice address:

_____
_____
_____
_____
_____

_____
Date, Signature **Stamp**

VAT no.: _____
(institutes / companies in EU countries only)

Purchase Order No.: _____

Credit Card Payment

VISA, MasterCard, AMERICAN EXPRESS
Please use the Credit Card Token Generator located at the website below to create a token for secure payment. The token will be used instead of your credit card number.

Credit Card Token Generator:
https://www.wiley-vch.de/editorial_production/index.php

Please transfer your token number to the space below.

Credit Card Token Number:

Cover Posters

Posters are available of all the published covers and frontispieces in two sizes

☐ DIN A2 42 x 60 cm / 17 x 24in (one copy: **39 Euro**)
☐ DIN A1 60 x 84 cm / 24 x 33in (one copy: **49 Euro**)

Postage for shipping posters overseas by airmail:
+ 25 Euro

Postage for shipping posters within Europe by surface mail:
+ 15 Euro

Price list for reprints (The prices include mailing and handling charges. All Wiley-VCH prices are exclusive of VAT)

No. of pages	Price (in Euro) for orders of 50 copies	100 copies	150 copies	200 copies	300 copies	500 copies
1-4	345	395	425	445	548	752
5-8	490	573	608	636	784	1077
9-12	640	739	786	824	1016	1396
13-16	780	900	958	1004	1237	1701
17-20	930	1070	1138	1196	1489	2022
for every additional 4 pages	147	169	175	188	231	315

★ **Special Offer** ★ If you order 200 or more reprints you will get a PDF file for half price.

Wiley-VCH Verlag GmbH & Co. KGaA; Location of the Company: Weinheim;
Chairman of the Supervisory Board: Stephen Michael Smith,
Trade Register: Mannheim, HRB 432833, General Partner: John Wiley & Sons GmbH,
Location: Weinheim, Trade Register Mannheim, HRB 432296,
Managing Director: Sabine Steinbach

WILEY-VCH

REVIEW

Carbon Capture

L. Zou, Y. Sun, S. Che, X. Yang, X. Wang, M. Bosch, Q. Wang, H. Li, M. Smith, S. Yuan, Z. Perry, H.-C. Zhou* .....x–xx

Porous Organic Polymers for Post-Combustion Carbon Capture

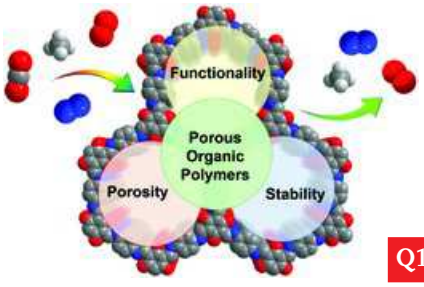

Significant progress has been made in the exploration of porous organic polymers (POPs) as potential porous solid adsorbents for carbon capture. A detailed correlation study between the structural and chemical features of POPs and their adsorption capacities is discussed, mainly focusing on physical interactions and chemical reactions.

Q1

ADVANCED MATERIALS
www.advmat.de

Porous Organic Polymers for Post-Combustion Carbon Capture

*Lanfang Zou, Yujia Sun, Sai Che, Xinyu Yang, Xuan Wang, Matheiu Bosch, Qi Wang, Hao Li, Mallory Smith, Shuai Yuan, Zachary Perry, and Hong-Cai Zhou**

One of the most pressing environmental concerns of our age is the escalating level of atmospheric CO_2. Intensive efforts have been made to investigate advanced porous materials, especially porous organic polymers (POPs), as one type of the most promising candidates for carbon capture due to their extremely high porosity, structural diversity, and physicochemical stability. This review provides a critical and in-depth analysis of recent POP research as it pertains to carbon capture. The definitions and terminologies commonly used to evaluate the performance of POPs for carbon capture, including CO_2 capacity, enthalpy, selectivity, and regeneration strategies, are summarized. A detailed correlation study between the structural and chemical features of POPs and their adsorption capacities is discussed, mainly focusing on the physical interactions and chemical reactions. Finally, a concise outlook for utilizing POPs for carbon capture is discussed, noting areas in which further work is needed to develop the next-generation POPs for practical applications.

Q2

1. Introduction

The CO_2 concentration in the atmosphere has increased dramatically in the past few decades and is held as one of the major causes for global warming.[1] Since the beginning of the industrial age, the CO_2 concentration has increased from 280 to 390 ppm in 2011, an increase of approximately 40%.[2] These emissions stem predominately from the burning of fossil fuels (coal, petroleum, and natural gas) and are projected to continue to increase in the foreseeable future.[3] Increases in the CO_2 concentration affects the incoming and outgoing energy in the atmosphere, resulting in a significant increase of the average atmospheric temperature. It is beyond all doubt that strategies to mitigate the increase of the CO_2 concentration in the atmosphere are urgently required.[4]

L. Zou, Y. Sun, S. Che, X. Yang, Dr. X. Wang, M. Bosch, Q. Wang, H. Li, M. Smith, S. Yuan, Z. Perry, Prof. H.-C. Zhou
Department of Chemistry
Texas A&M University
College Station, Texas, 77842-3012, USA
Prof. H.-C. Zhou
Department of Materials Science and Engineering
Texas A&M University
College Station, Texas, 77843, USA
Q3
Correspondence to: Prof. H.-C. Zhou (E-mail: zhou@chem.tamu.edu)
The ORCID identification number(s) for the author(s) of this article can be found under http://dx.doi.org/10.1002/adma.201700229

DOI: 10.1002/adma.201700229

Carbon capture and storage (CCS)[5] is a family of technologies that can reduce CO_2 emissions.[6,7] CCS includes three steps: a) separation of CO_2 from emission sources before entering the atmosphere (carbon capture); b) transportation to a storage site; and c) permanent subterranean or submarine storage. In the latter two steps, captured CO_2 is pressurized to ≈100 bar or more and transported to a storage site, where it is injected and trapped underground for hundreds to thousands of years. So far, a growing number of fully integrated CCS projects have reached pilot prior to commercialization. However, the large energy penalty and considerable cost of the carbon capture process are slowing down the deployment of commercial CCS projects.

1.1. Carbon Capture Scenarios

Exploring cost-effective and scalable technologies for carbon capture from emission sources is regarded as one of the most efficient strategies to reduce anthropogenic CO_2 emissions.[8] Generally, based on the fundamental chemical process involved in the combustion of fossil fuels, three basic CO_2 capture scenarios can be adopted: a) post-combustion capture, b) pre-combustion capture, and c) oxy-fuel combustion.[9,10] In addition, the carbon capture used for CH_4 purification and direct air capture will also be discussed.

1.1.1. Post-Combustion Capture

The goal of the post-combustion process is to separate CO_2 from N_2 after combustion of fossil fuels before it enters the atmosphere. The combustion of fossil fuels in air generates flue gas

consisting of 15% CO_2, majority N_2, and other minor components such as H_2O, CO, NO_x, and SO_x (**Table 1**).[11] After the removal of SO_x, flue gas enters the carbon capture process at near atmospheric pressures and elevated temperatures (40–80 °C).[12–14] This carbon-capture scenario is the most feasible on a short time scale since many of the proposed technologies can be retrofitted to the existing fossil fuel consuming power plants.

1.1.2. Pre-Combustion Capture

In pre-combustion capture, a primary fuel reacts with oxygen or air, producing synthesis gas (syngas), mainly composed of CO and H_2. Then CO passes through a shift converter and reacts with steam to produce CO_2 (25%–35%) and additional H_2 (30%–50%) at high pressure (5–40 bar) in the catalytic reactor (Table 1). Therefore, the target in pre-combustion is to separate CO_2 from H_2.[15] The capture usually operates at elevated pressures (≈30 bar) and temperatures (≈40 °C) with an adsorbent bed. A pressure drop is later applied to recycle those adsorbents.[10,16] The energy requirement of this pressure swing adsorption (PSA) cycle is low. However, the temperature and efficiency associated with H_2-rich turbine fuel are problematic.

1.1.3. Oxy-Fuel Combustion

In a conventional oxy-fuel combustion setup, nearly pure oxygen is fed into the plant and diluted with CO_2 from the flue steam to a partial pressure of 0.21 bar. In this way, not only can the temperature of the fuel combustion be easily controlled, but also the NO_x impurity can be reduced when coal is burned in an O_2-enriched atmosphere.[17] The gaseous product contains mainly CO_2 (55%–65%) and H_2O (25%–35%). After condensation and water removal, nearly pure CO_2 can be directly subjected to sequestration.[18] While pre-combustion and post-combustion capture cannot be easily implanted into industry, 95% of carbon capture processes have been achieved by oxy-fuel combustion.[19] One significant advantage of this process is that flue gas is almost entirely composed of CO_2, which greatly benefits the following separation process. Most existing power plants can be readily retrofitted with an oxy-fuel combustion system. However, the stringent requirement for nearly pure oxygen significantly enhances the cost, making the implementation of oxy-fuel combustion challenging.

1.1.4. CH_4 Purification

Carbon capture can also be utilized for natural gas purification (mainly CH_4).[20,21] When natural gas is extracted from wells, it often contains 20–40 wt% of CO_2, which is generally vented to the atmosphere. The significant challenge in this separation is the special technologies and materials are required to withstand high pressures during extraction of natural gas.

1.1.5. Direct Carbon Capture

The target here is to separate CO_2 directly from the atmosphere, where CO_2 is highly dilute with a partial pressure of 400 ppm. Until now, relatively few adsorbents have demonstrated effective abilities to remove CO_2 through direct sequestration.[22] However, carbon capture in enclosed environments, such as submarines and aircraft, have been reported using materials including supported poly(ethylene imine) or poly(ethylene glycol).

Lanfang Zou obtained her B.S. degree from Nanjing University in 2012. She joined Texas A&M University in the same year, obtaining her Ph.D. in chemistry in 2017 under the guidance of Prof. Hong-Cai Zhou. Her work is focused on the synthesis and functionalization of novel stable metal-organic frameworks (MOFs) and porous polymer networks (PPNs) for practical applications, such as gas storage, gas separation, and heterogeneous catalysis.

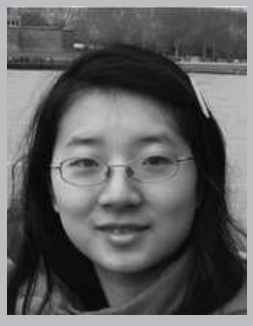

Yujia Sun obtained her B.S. degree in 2013 from Wuhan University, where she worked on organic synthesis methodology. Then, she joined Dr. Hong-Cai Zhou's group as a Ph.D. student at Texas A&M University. Her research interest is focused on the synthesis of functional porous materials (PPNs and MOFs) and their applications.

Hong-Cai "Joe" Zhou obtained his Ph.D. in 2000 from Texas A&M University. After a postdoctoral stint at Harvard University, he joined the faculty of Miami University, Oxford in 2002. He moved back to Texas A&M University in 2008. He was promoted to Davidson Professor of Science in 2014 and a Robert A. Welch Chair in Chemistry in 2015. His research focuses on the discovery of synthetic methods to obtain robust framework materials with unique catalytic activities or desirable properties for clean-energy-related applications.

Table 1. Benchmark parameters showing typical compositions of gases (vol%) in post-combustion, pre-combustion and methane reformation processes as well as several physical parameters relevant to carbon capture.[10]

	Post-combustion	Pre-combustion[a)]	Kinetic Diameter (Å)	Quadrupole moment[b)]
CO_2	15–16%	25–35%	3.30	43.0
N_2	70–75%	0.3–2.3%	3.64	15.2
H_2	–	30–50%	2.89	6.62
H_2O	5–7%	15–40%	2.65	–
O_2	3–4%	–	3.45	3.9
CO	20 ppm	0.5–0.7%	3.75	25.0
SO_x	800 ppm	–	–	–
NO_x	500 ppm	–	–	–
H_2S	–	0.1–0.2%	3.60	–

[a)] Before water-gas shift reaction. [b)] 10^{-27}esu^{-1} cm^{-1}.

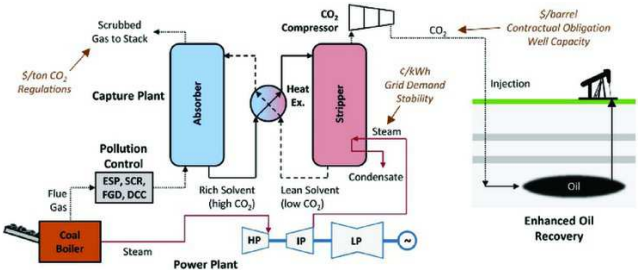

Figure 1. Carbon separation schematic for a coal fired power plant with flue gas CO_2 capture to EOR operations. Reproduced with permission.[25] Copyright 2016, American Chemical Society.

1.2. Currently Used Materials

All large-scale commercial CO_2 capture systems rely on the basic premise of the original patent, wherein some base dispersed in an aqueous solution binds to acidic gases present in the flue gas stream (**Figure 1**). Hundreds of plants operate on these systems with more coming on-line in the future.[23] The process involves the absorption of CO_2 into an aqueous solution of amine with low volatility at ambient temperature and the regeneration of amine by stripping with water vapor at 100 °C to 120 °C. Aqueous amine solutions, however, have several major drawbacks, which have generally made them uneconomical for implementation in existing power plants.[24] Engineering and system design concerns of the typical corrosiveness of amine solutions and vapors means that costly designs must be implemented for longevity, and frequent housekeeping is necessary to keep the system running safely.[25] The volatility and stability of some amines also pose problems in material lifetime, requiring additives and recharging of amines that are lost or oxidized.[26–28] In addition, the parasitic energy costs associated with stripping CO_2 from the sorbents can divert 20%–30% of generated energy towards the capture process, resulting in the largest economic barrier.[29,30] Therefore, commercial amine systems have been developing other approaches to tackle the problems inherent involved with aqueous amine capture.[31–36]

As an alternative, porous solid materials have been demonstrated as potential media for carbon capture,[37–40] including zeolites,[41–48] porous carbons,[49–55] and silica.[56–60] Carbon capture by traditional sorbents, such as zeolites and porous carbons, is much more energy efficient as compared to aqueous amine solutions. First, the absence of new chemical bonds formation between the sorbates and sorbents leads to significantly less energy demands for regeneration. In addition, the heat capacities of sorbents are only a fraction of that of the amine solution, further reducing the energetic costs involved with heating aqueous solutions.[61] However, the porous carbons are limited by low CO_2/N_2 selectivities, while zeolites suffer from impaired performance in the presence of water.[62,63] Therefore, there is an urgent need to develop advanced sorbents with excellent CO_2/N_2 selectivity, high CO_2 capacity, and enduring performance under flue gas conditions.

More recently, metal–organic frameworks (MOFs) have garnered a significant amount of attention as porous materials for carbon capture.[9,10,64–73] MOFs comprise metal-containing nodes and organic linkers that are assembled through coordination bonds. They have geometrically and crystallographically well-defined structures and in many cases, these structures are robust enough to allow the removal of included guest species, resulting in permanent porosity. The crystallinity of MOFs also allows precise structural characterization by diffraction methods, thus facilitating their rational design and the formulation of structure–function relationships. Such remarkable and easy tunability is quite different from those of traditional porous materials, such as zeolites and activated carbon. However, constructed with soft Lewis acids and hard Lewis bases, MOF materials usually suffer from limited physicochemical stability.

Porous organic polymers (POPs) are composed predominantly of carbon, boron, oxygen, and nitrogen that are connected through strong covalent bonds.[74–79] A significant number of POPs have been studied for carbon capture, some of which have demonstrated promising performances.[16,65] The major advantages of POPs over other porous materials are their high porosity, structural diversity, and ultrahigh physicochemical stability, the combination of which enables an enormous scope of postsynthetic modifications to introduce specific CO_2-philic functionalities. In general, POPs can be handled under standard wet chemical reaction conditions without significant degradation of

the framework or loss of porosity, and are ideal for applications in capturing CO_2 from harsh flue gas conditions.

1.3. Porous Organic Polymers

POPs are a new category of hyper-crosslinked polymeric materials constructed exclusively from organic covalent bonds.[80–84] POPs can be successfully synthesized by incorporating multitopic monomers, which provide cross-links between propagating polymer chains, into well-known step-growth and chain-growth polymerizations. POP materials have been used in many potential and important applications, such as gas adsorption,[85–87] gas separation,[88,89] optoelectronics,[90–95] catalysis,[96–99] proton conductivity,[100] chemical sensors,[101–103] drug delivery,[104] and energy storage.[105,106] Different types of POPs have been denoted by various names, including porous polymer networks (PPNs),[107–110] porous organic frameworks (POFs),[111,112] conjugated microporous polymers (CMPs),[113–115] polymers of intrinsic microporosity (PIMs),[116–120] hypercrosslinked polymers (HCP),[121–124] covalent triazine-based frameworks (CTFs),[125,126] porous aromatic frameworks (PAFs),[77,107,127] crystalline covalent organic frameworks (COFs)[76,128] and so on. For convenience, we will use the term POPs to broadly label these materials.

Using POPs as carbon capture materials has the following principal advantages: a) constructed from comparatively rigid monomers, POPs can yield pores with rigid walls, leading to permanent porosity. The surface areas of POPs are comparable to the most porous materials. In particular, PPN-4, made by linking tetrakis(phenyl) subunits using Yamamoto coupling, has demonstrated the highest Brunauer–Emmett–Teller (BET) surface areas (6461 $m^2\ g^{-1}$) among all POP materials published so far.[107] b) The synthesis of POPs have drawn from an enormous number of modern bond-forming methodologies, including boronic acid condensation,[76,128,129] metal-catalyzed coupling,[107,109,130,131] imine formation,[132–136] Friedel–Crafts alkylation,[126,137] and so on. The assembly process of POPs combines merits of the enormous reaction choices and rational design of monomers, leading to numerous structural topologies and diversified porosities. c) POPs, composed of light elements (typically H, B, C, N, and O), are usually lightweight materials; therefore, their gravimetric carbon capture capacities tend to be higher. d) Due to the nature of covalent bonds, POPs usually have very high stability compared with most MOFs, which are linked through coordination bonds.[135,136] Their exceptional chemical and water stability enable their reusability. The combination of favorable properties of large surface area, tunable pore size, high stability and easy functionalization enable POPs as ideal candidates for carbon capture. Although some excellent reviews have already documented the synthesis and application of POPs,[66,138–142] very few have focused on the developments and achievements of POP materials for carbon capture.[16,65]

This review is intended to provide readers with a comprehensive overview of the considerations associated with carbon capture using POPs. First, various definitions and terminologies used to evaluate the performance of POPs for carbon capture, including the CO_2 capacity, enthalpy of CO_2 adsorption, selectivity and frequently used regeneration strategies are introduced in Section 2. A detailed correlation study between the structural and chemical features of POPs and their adsorption capacities will also be discussed, focusing on their physical interactions (Section 3) and chemical reactions (Section 4). Ultrahigh-surface-area POPs usually have weak physical interactions with CO_2 molecules, and they could find use in pre-combustion carbon capture, where the processes operate at elevated pressures.[69,143–145] Chemical functionalization of POPs with polar groups, including nitrogen-rich groups,[146–150] oxygen-rich groups,[113,137,151] and inorganic ions,[110,152–155] can be utilized to enhance the average dipole-quadruple interactions with CO_2 with a result of improved CO_2 capacity. Moreover, alkyl-amine functionalized POPs can undergo chemical reactions with CO_2 and therefore tend to have higher adsorption enthalpies and selectivities.[109,156–158] Such materials have great potential for practical applications in post-combustion carbon capture. Finally, a concise outlook for utilizing POPs for carbon capture will be discussed in Section 5, noting areas in which further work is needed to develop the next-generation POPs for practical applications. The current challenges toward using POPs in CO_2 capture will be outlined clearly so that the relevant scientific fields can move the conversation forward towards practical solutions.

2. Definitions and Terminologies Used in Carbon Capture

Essential criteria to evaluate the performance of POPs for carbon capture includes CO_2 uptake capacity, CO_2 selectivity over other gases, regeneration energy, recyclability and stability under the carbon capture condition atmosphere.[62] Hence, there is a great need to standardize the terminology used before exploring the carbon capture properties of POPs.

2.1. Porosity, Surface Area and CO_2 capacity

Porosity is an important factor affecting the adsorptive performance of POPs. The surface areas of POPs are typically analyzed using BET theory,[159] which is based on multi-layer adsorption and is an extension of Langmuir theory,[160] a theory focusing on monolayer adsorption. The BET theory in most cases uses N_2 as a probe to quantify gas adsorption properties over a wide range of pressures at constant temperature, and surface area is eventually determined according to an adsorption isotherm.[161] Rouquerol plots are utilized to determine the linear range of the BET plot for microporous materials to improve the accuracy of the calculated BET surface area.[162]

CO_2 uptake in porous materials is sensitive to the pore dimensions. High volumetric uptake is generally observed in a microporous material (smaller than 2 nm) due to the similarity in pore dimensions to the kinetic diameter of CO_2 molecules. The pore size distribution is commonly determined semi-empirically by combining the experimental N_2 isotherm with non-linear density functional theory (NLDFT).[163–165] If irreversible reactions are utilized to synthesize the POPs, they are generally amorphous with broader pore size distributions,[101,117,118] compared to those of MOFs[166–169] and COFs,[86,170,171] which undergo self-correcting processes to form highly crystalline structures.

The adsorption capacity, a critical parameter to evaluate the working performance of the material, can be expressed in both volumetric and gravimetric terms. The gravimetric capacity, defined as the amount of CO_2 adsorbed per unit mass of adsorbent is typically expressed in units of mmol per gram (mmol g^{-1}), gram per gram (g g^{-1}), or weight percent (wt%). The volumetric capacity, related with how densely the CO_2 can be stored within the materials, is the volume of CO_2 adsorbed per volume unit of adsorbent (cm^3 cm^{-3}, L L^{-1}). The capacity is typically determined by gas adsorption. The volumetric capacity can be converted to the gravimetric capacity using the densities of the gas and the material. Both the gravimetric and volumetric capacities are crucial in determining the mass and volume of the adsorbent bed required to store a given amount of CO_2.

2.2. Enthalpy of Adsorption

The enthalpy of CO_2 adsorption is another significant parameter to evaluate the performance for CO_2 capture. As gas adsorption is the result of the attractive interaction between adsorbate and adsorbent, the enthalpy of adsorption can reflect the affinity between pore surface and gas molecules, which also affects the adsorptive selectivity and the energy required to regenerate the materials. When designing and synthesizing the POPs, it is important to optimize the binding force so as to balance the selectivity and the regeneration energy. For example, one material, in which the CO_2 molecule binds with the pore surface tightly, will show high CO_2 selectivity. However, the tightly bound CO_2 also increases the amount of energy for regeneration, which are necessary to break the strong interactions between POPs and CO_2. Conversely, as the enthalpy of adsorption decreases, the energetic cost to recycle the materials also decreases, however, the adsorptive selectivity will also be decreased.

Quantitatively, the isosteric heat of adsorption (Q_{st}) is used to represent the enthalpy of CO_2 adsorption. The Q_{st} is the average enthalpy of adsorption for a gas molecule at different binding sites determined at a specific coverage. Generally, isotherms collected at two different temperatures are used to calculate the Q_{st} of CO_2 adsorption. However, the readers are encouraged to use at least three different temperatures in order to accurately calculate Q_{st} values. The isotherm data first needs to be fitted with a virial-type equation[172] Q6

$$\ln P = \ln N + \frac{1}{T}\sum_{i=0}^{m} a_i N^i + \sum_{j=0}^{n} b_j N^j \tag{1}$$

where a_i and b_j are virial coefficients of the component, P is the pressure, N is the absorbed amount of gas, T is temperature, and m and n are the number of virial coefficients required to adequately describe the isotherms.

Q_{st} can then be calculated by using the Clausius–Clapeyron equations,[173]

$$\ln P = \frac{-Q_{st}}{RT} + C \tag{2}$$

$$\frac{-Q_{st}}{R}\cdot\frac{1}{T} + C = \frac{1}{T}\sum_{i=0}^{m} a_i N^i + \ln N + \sum_{j=0}^{n} b_j N^j \tag{3}$$

$$Q_{st} = -R\sum_{i=0}^{m} a_i N^i \tag{4}$$

where P is pressure, T is the temperature, R is the universal gas constant (8.314 J K^{-1} mol^{-1}), and C is a constant.

Another way to calculate Q_{st} is to use the Langmuir model. First the measured experimental data on pure component isotherms, in terms of excess loadings, are converted to absolute loading using the Peng–Robinson equation of state for estimation of the fluid densities. Then the absolute component loadings are fitted with single-site or dual-site Langmuir model based on the isotherm inflections. If there is no discernible isotherm inflection, the isotherm data will be fitted with single-site Langmuir model

$$q = \frac{q_{sat} b p}{1 + bp} \tag{5}$$

where b is the parameter in the pure component Langmuir adsorption isotherm, q is molar loading of adsorbate, q_{sat} is saturation loading.

If there are isotherm inflections, the dual-site Langmuir model will be used to fit the isotherm data

$$q = q_A + q_B = \frac{q_{sat,A} b p}{1 + q_{sat,A} b p} + \frac{q_{sat,B} b p}{1 + q_{sat,B} b p} \tag{6}$$

Then the isosteric heat of adsorption, Q_{st}, can be calculated using

$$Q_{st} = RT^2\left(\frac{\partial \ln p}{\partial T}\right)_q \tag{7}$$

and the detail analytic procedures are provided in the ESI of the paper Mason et al.[280]

The strength between CO_2 molecules and binding sites in POPs can also be measured by the zero-coverage isosteric heat of adsorption. Commonly, Q_{st} will decrease with increasing coverage of adsorbate, thus, the zero-coverage isosteric heat of adsorption indicates the strongest binding sites in the materials. Based on the magnitude of Q_{st}, we can attribute adsorption processes to specific chemical features of the pore surface, such as open metal sites or amine functionalities. By using Equation (4), the zero-coverage isosteric heat of adsorption when $N = 0$ is calculated

$$Q_{st} = -Ra_0 \tag{8}$$

The magnitude of Q_{st} is also indicative of the nature of the adsorption process. Adsorption of CO_2 can occur by either physisorption or chemisorption. Physisorption occurs through the weak van der Waals interactions between the adsorbate and adsorbent. The quadrupole of CO_2 makes it sensitive to polar groups at the pore surface, and thus functionalization of the interior provides a way to finely tune the interactions of CO_2 with the adsorbent. Chemisorption involves the formation of chemical or ionic bonds. The bond-forming character of chemisorptive processes cause greater enthalpy changes, and thus a larger magnitude of Q_{st} values. In particular, alkylamine functionalities have been long known to react with CO_2 to form carbamates in a reversible fashion. The value of Q_{st} will also govern the amount of energy required to regenerate a given material. If the interactions between CO_2 and the adsorbent are enthalpically favorable, such as the case for carbamate formation from alkyl amines, Q_{st} will be large.[62] As the magnitude of Q_{st} increases, the amount of energy needed to reverse bond formation and regenerate the material increases, and consequently so does the cost. Lowing of the Q_{st} values will reduce the costs of regeneration, but could potentially negatively affect the selectivity of CO_2 over other components in a gas mixture as the values will begin to approach that of other gases, such as N_2 and CH_4, which have lower affinities for polarized surfaces than CO_2, and lower Q_{st} values.

CO_2 capacity and adsorption enthalpy are two vital properties for evaluating the performance of adsorbents in carbon capture. Adsorbents with high CO_2 capacity and low enthalpy are particularly attractive. Dai and co-workers have established knowledge of the relationships between CO_2 capacity and enthalpy in the chemical absorption of CO_2 through combining the van't Hoff equation with the reaction equilibrium thermodynamic model (RETM). The variations of capacity with enthalpy change were found to be distinctively sigmoid functions and these calculated variation curves agrees well with the experimental results.

2.3. Selectivity

A high selectivity for CO_2 over other gas components (such as N_2, H_2, CH_4) is essential in both pre-combustion and post-combustion carbon capture processes. There are two primary mechanisms of selectivity. The first mechanism is the kinetic control process, also known as the size-exclusion process, where molecules are excluded from diffusing into a pore based on differences in their kinetic diameter (Table 1). For CO_2/N_2 separations, the similar kinetic diameter of these two gases (CO_2, 3.3 Å; N_2, 3.64 Å) mandates that CCS materials must possess very small pores and narrow pore size distributions in order to exclusively trap CO_2. The second mechanism of separation is a thermodynamic approach and is based on the different binding affinities between the pore surface and the adsorbates. For this adsorption mechanism, the separation of gas mixtures depend primarily on the physical properties of gas molecules. The higher polarizability (CO_2, 29.1×10^{-25} cm^{-3}; N_2, 17.4×10^{-25} cm^{-3}) and quadrupole moment (CO_2, 13.4×10^{-40} $C{\cdot}m^2$; N_2, 4.7×10^{-40} $C{\cdot}m^2$) of CO_2 compared with N_2 results in a higher affinity of the pore surface for CO_2, which plays a vital role in separation of CO_2/N_2.

It is important to address how to determine the selectivity factor of a binary mixture. It is not convenient to collect the isotherm data by directly testing the adsorption of a mixed component gas. Therefore, it is important to choose a suitable adsorption model, such as Henry's law or ideal adsorbed solution theory (IAST), to calculate the adsorption selectivity by using single-component isotherm data.

2.3.1. Henry's Law

In order to use Henry's Law to determine the selectivity of CO_2 over other gases, isotherm data must be fit using a non-linear virial-type equation (Equation (1)).[175] The Henry's constant (K_H) can be calculated from the values of virial coefficients a_0 and b_0 by using Equation (9), where T is temperature.

$$K_H = \exp(-b_0) \cdot \exp(-a_0/T) \tag{9}$$

The selectivity of CO_2 (i) over other component (j) can then be estimated by calculating the ratio of Henry's constants

$$S_{ij} = \frac{K_{Hi}}{K_{Hj}} \tag{10}$$

2.3.2. Ideal Adsorbed Solution Theory (IAST)

Another way to determine the adsorptive selectivity is the ideal adsorbed solution theory (IAST), which was put forward by Myers and Prausnitz.[176] IAST has been demonstrated as a viable method to calculate selectivities that are in good agreement with selectivity calculated from gas mixtures for a variety of POPs.[177,178] The validity of this method rests on three assumptions: 1) the adsorbents must be thermodynamically inert, meaning that any fluctuation in thermodynamic properties of adsorbents should be negligible during the adsorption process; 2) the surface area of adsorbents must be temperature-invariable and constant for all adsorbates; 3) the gas components must behave as ideal gas.

To apply IAST to modeling adsorption of gas mixtures, the first step is to fit the experimental single-component isotherms by single-site or dual-site Langmuir–Freundlich model

$$q_i = \sum_{i=1}^{n} q_{i,sat} \frac{b_i p^{v_i}}{1 + b_i p^{v_i}} \tag{11}$$

where $q_{i,sat}$ is the saturation capacity of species i, b_i is the Langmuir–Freundlich constant for species i, p is the gas phase pressure of species i.

The adsorption selectivity for binary mixture is defined by Equation (12) and the calculation is performed for binary mixtures with equal partial pressures in the gas phase.

$$S = \frac{q_1/q_2}{p_1/p_2} \tag{12}$$

where q_i is the molar loading of component i, and p_i is the gas phase pressure of component i.

Optimal selectivity for CO_2 uptake for a material depends on the target application. Pre-combustion separation is important for the separation of CO_2 from H_2 that is generated by the water-gas shift reaction of syngas. Highly selective adsorbents are especially desired in the large-scale production of H_2 for the use in hydrogen fuel cells required high H_2 purity. The pre-combustion process is generally carried out at an elevated pressure with CO_2 concentrations greater than 15%. Therefore, the adsorbent material needs to exhibit selective adsorption of CO_2 over H_2 under high-pressure conditions for effective pre-combustion separation. In post-combustion separation, CO_2 is removed from a stream of industrial flue gas consisting of primarily N_2 and CO_2. The concentration of CO_2 in flue gas is low, generally ≈15% ($v\ v^{-1}$) at ambient conditions. A high selectivity for CO_2 over N_2 at low pressure is desired for adsorption of CO_2 from flue gas. In addition, CO_2 extraction from natural gas is an important industrial process that requires materials with selective adsorption of CO_2 over CH_4. Therefore, depending on the selectivity requirements of the targeted application, the physical properties of POPs can be tuned to maximize CO_2 uptake and adsorbent efficiency.

2.3.3. Breakthrough Experiments

After discussing how to use different models to calculate adsorptive selectivity from single-component gas adsorption isotherms, we will now focus on evaluation of the performance of gas separation experimentally. The fixed-bed breakthrough experiment is a straightforward way to mimic the adsorption of a real mixed gas.[110,179,180] In a common setup, the gas inlets connect to the adsorbent bed by flow controllers so that the composition of the gas mixture can be controlled. The gas mixture passes through packed beds of the solid adsorbent while the output gas is monitored by detection methods, such as mass spectrometry (MS) or gas chromatography (GC). For a system that preferentially binds CO_2, the output concentration of CO_2 is zero prior to saturation of binding sites with guest molecules. Once the material is saturated, the output concentration of CO_2 will increase sharply, corresponding to the breakthrough time, and the components will eventually achieve a constant concentration. The breakthrough time describes the time it takes to completely saturate a material's adsorption sites, and can be plotted against the concentration of component gases to obtain a breakthrough curve. Under the same measurement condition, longer breakthrough times suggests for higher CO_2 capacity. In addition, molar fraction (concentration) of the component gases is an important parameter to evaluate the selectivity of the material over different gases. The breakthrough experiments provide an excellent way to simulate the conditions of post-combustion CO_2 separation from industrial flue gas in a laboratory setting.

2.4. Recyclability

Recyclability is important in determining the practicality and economic feasibility of using POPs for large-scale CO_2 capture.[181,182] Recyclability can be assessed in the laboratory by monitoring the CO_2 uptake over many cycles of adsorption/desorption and regeneration. In practical, there are many methods of regeneration, which can be used individually or in combination, including: 1) increase in temperature; 2) reduction in partial pressure; 3) reduction in concentration of CO_2; 4) purge with an inert gas flow; 5) displacement with a more strongly adsorbing species; 6) change of chemical conditions.

The regenerability of POPs can approached by typical adsorption methods employed in the activation of porous materials that are based on manipulating temperature and pressure conditions. Pressure swing adsorption (PSA) is an isothermal process where evacuation of a high-pressure stream to achieve ambient pressures is used to regenerate a sorbent.[183] In the case of pressures lower than atmospheric pressure, vacuum swing adsorption (VSA) is used. VSA becomes less applicable for large scale industrialization due to energetic costs of powering a vacuum system. At high pressures, gas molecules favor interactions with the adsorbents, and the strength of these interactions depends on the adsorbing species. Upon lowering the pressure, molecules bind to the surface of the adsorbent more weakly, and can be selectively removed based on their individual affinities to the surface at a given pressure. In a temperature swing adsorption (TSA) regeneration process, desorption is promoted by passage of a hot stream of gas through the adsorbent bed.[184,185] Elevated temperatures raise the internal energy of adsorbate molecules, allowing them to escape from the adsorbent surface. As a result, TSA methods can easily become energetically costly as the required desorption temperature increases and ultimately are most applicable for desorption of CO_2 at low concentrations. However, TSA is unsuitable for materials undergoing thermal decomposition prior to achieving desorption temperatures.

Recently, a novel method referred to as moisture swing adsorption (MSA) has been applied to adsorbent regeneration.[186,187] In the MSA process, adsorbents bind CO_2 under dry conditions and release CO_2 in the presence of moisture. The MSA method mechanism was first demonstrated on an anionic exchange resin, as shown **Figure 2**. First, carbonate ions interact strongly with the limited amount of water present on the surface of a dry resin, leading to the formation of bicarbonate ions and hydroxide ions (Transition from Empty–Wet to Empty–Dry). The hydroxide ions that are formed provide sites for CO_2 capture, leading to the formation of another bicarbonate ion (Transition from Empty–Dry to Full–Dry). When the saturated material comes in contact with moisture, the neighboring bicarbonate ions interact with each other through hydrogen bonding between water molecules (Transition from Full–Dry to Full–Wet). Finally, CO_2 is released from the surface upon the formation of carbonate ions (Transition from Full–Wet to Empty–Wet). The process is ideal because of the low cost of water and absence of applied heat. Above all, regeneration strategies must be designed to minimize the total cost of capturing CO_2, and as such, there will be a trade-off between maximizing the working capacity and minimizing the energy required for regeneration.

In order to form part of an economically viable process, an ideal adsorbent must have large CO_2 sorption capacity. It must also have good selectivity of CO_2 with respect to other gas components to generate a CO_2 steam of the required purity, suggesting that CO_2 must be adsorbed strongly enough to facilitate the separation. Meanwhile, the interaction cannot be too strong as to avoid generating extra energy penalties in the regeneration

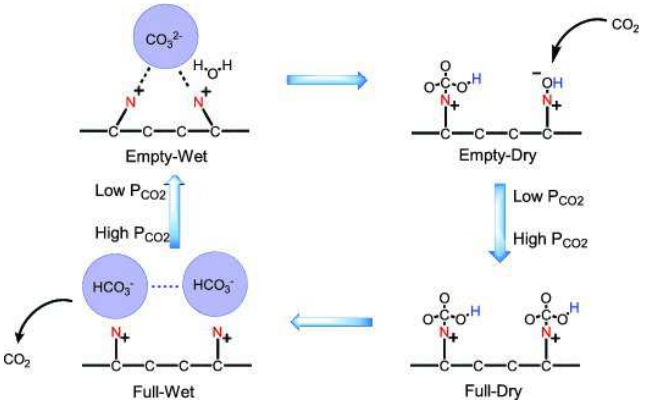

Figure 2. Reaction path of CO_2 adsorption and desorption during a moisture swing.

process. Additionally, a candidate adsorbent is also expected to have good physicochemical stability, including moisture, thermal, and chemical stability. Finally, candidate materials must be synthesized from low cost monomers and polymerizations, with easily scalable preparations.

3. Carbon Capture in Porous Organic Polymers based on Physical Interactions

POPs have been proven to be a material of great potential in carbon capture applications, which can be attributed to their large permanent surface areas, suitable pore size distributions, and suitable interactions with carbon dioxide.[188] The CO_2 uptake capacities at 1 bar and 273 K, the CO_2 uptake capacities at 1 bar and 298 K, the CO_2 uptake capacities at 0.15 bar and 298 K, CO_2/N_2 selectivity and heats of adsorption for selected POPs are listed in **Table 2**. Note that some data have been taken approximately from the figures or curves published in the literature. Many POPs exhibit good performances for carbon capture at 1 bar and 273 K/298 K. Notably, it is important to address the conditions relevant to the post-combustion carbon capture process of CO_2 (0.15 bar, 40 °C). We urge that these pressure and temperature conditions be implemented as standard conditions in future reports of CO_2 adsorbent testing in order to effectively evaluate their applicability to post-combustion carbon capture and expedite the design and discovery process.

CO_2 adsorption is a well-established CO_2 separation approach used in the chemical and petroleum industries today. Adsorbents typically fall into either of two categories: 1) physical adsorption, which is temperature and pressure dependent (adsorption occurs at high pressures and low temperatures) and 2) chemical adsorption, where adsorption of CO_2 depends on the acid–base neutralization reaction.[189] For the physical adsorption mechanism, the separation of gas mixtures mainly depends on the physical properties of gas molecules, as discussed previously in Section 2.3. Materials that physically adsorb CO_2 usually consume less energy to regenerate because lack of new bond formation between the adsorbate and sorbent, as in the case of chemisorption. Even though surface area can affect the CO_2 uptake, it is definitely not the dominant reason, especially for post-combustion carbon capture (at low pressure and high temperature). Instead, the functionalization of POPs plays a vital important role in the post-combustion CO_2 uptake properties. Hence, chemical functionalization of POPs with polar groups can be utilized to enhance the average dipole-quadruple interactions with carbon dioxide, leading to higher carbon-capture capacity as well as higher selectivity.

3.1. Non-Functionalized Porous Organic Polymers

To date, a number of different types of coupling reactions and monomers have been successfully applied to synthesize various POPs. POPs with ultrahigh surface area usually have very weak physical interactions with CO_2 molecules and are thus applicable as materials in pre-combustion carbon capture. Among them, porous materials constructed from boron–oxygen bonds are among the first-reported and well-studied systems, often known as COFs.[74,128,221–223] Diboronic acids undergo condensation reactions, such as cyclotrimerization or reactions with orthobenzenediol moieties to form six or five-membered rings that lend to network formation.[128] Since boroxine ring formation is quite reversible, such COFs typically have good crystallinity with long-range order, making it possible to precisely design new COFs with atomic-level control. Moreover, boroxine ring-based COFs usually have a narrow pore-size distribution compared with amorphous porous materials. Unfortunately, the boroxine rings show relatively high sensitivities to moisture, which results in framework decomposition and reformation of boronic acids. As a result, boroxine-linked COFs may not be appropriate materials for post-combustion CO_2 capture. The introduction of specific functional groups onto the surface of such COFs, either by using pre-synthetic monomer or post-functionalization, may improve their water stability or enable their application in high-pressure CO_2 separation.[224–228]

Unlike the moisture sensitive nature of boroxine rings, polymers based on carbon–carbon bonds are relatively stable. Common strategies, such as Suzuki coupling,[212,229] Sonogashira reaction,[143,230–232] Yamamoto reaction,[75,107,145,154,233] Eglinton coupling,[79,234] and Friedel–Crafts reaction,[235,236] give rise to carbon–carbon coupling to produce amorphous solids. One of the current benchmark polymers for carbon capture is PPN-6,[154] also known as PAF-1.[75] The irreversible nature of carbon–carbon bond formation precludes the formation of structures with long-range order. Structural disorder and defects lead to relatively broad powder X-ray diffraction (PXRD) peaks and pore-size distributions. These materials have the potential to be applied in carbon capture due to their extraordinary chemical and thermal stabilities, large surface areas, and low cost. It must be pointed out that the synthetic conditions, such as solvent, temperature, and polymerization routes can have a major influence on the textural and gas uptake properties of POPs.[237] For example, the Cooper group initially demonstrated that the choice of reaction solvent can greatly affect the surface area and pore volume in POPs and should be a prime factor in the synthesis of new POPs.[232] In addition, the activation method and special treatment can play an important role in the gas adsorption properties of POPs.

Table 2. Summary of low-pressure CO_2 uptakes, CO_2/N_2 selectivity and heats of adsorption in selected POPs.

POPs	Main functional group	BET (m^2g^{-1})	CO_2 (mmol g^{-1}) 1bar, 273K	CO_2 (mmol g^{-1}) 1bar, 298K	CO_2 (mmol g^{-1}) 0.15bar, 298K	CO_2/N_2 Selectivity[a)] IAST	CO_2/N_2 Selectivity[a)] Henry's law	ΔH_{CO2} ($kJmol^{-1}$)	Ref.
COF-1	None functional	750	2.23	–	–	–	–	–	[69]
COF-5	None functional	1670	1.34	–	–	–	–	–	[69]
COF-6	None functional	750	1.40	–	–	–	–	–	[69]
COF-8	None functional	1350	1.22	–	–	–	–	–	[69]
COF-10	None functional	1760	1.02	–	–	–	–	–	[69]
COF-102	None functional	3620	1.38	–	–	–	–	–	[69]
COF-103	None functional	3530	1.39	–	–	–	–	–	[69]
BILP-1	Benzimidazole	1172	4.27	2.97	0.69	–	36	26.5	[190]
BILP-2	Benzimidazole	708	3.38	2.36	–	–	71	28.6	[149]
BILP-3	Benzimidazole	1306	5.11	3.00	1.02	–	31	28.6	[191]
BILP-4	Benzimidazole	1135	5.34	3.59	–	–	32	28.7	[149]
BILP-5	Benzimidazole	599	2.91	1.98	–	–	36	28.8	[149]
BILP-6	Benzimidazole	1261	5.00	2.84	1.07	–	39	28.4	[191]
BILP-7	Benzimidazole	1122	4.39	2.77	–	–	34	27.8	[149]
BILP-10	Benzimidazole	787	4.09	2.55	0.73	57	–	38.2	[192]
BILP-11	Benzimidazole	658	3.09	2.00	0.61	56	–	32.0	[192]
BILP-12	Benzimidazole	1497	5.07	3.18	0.72	31	–	27.6	[192]
BILP-13	Benzimidazole	677	2.57	1.79	0.43	32	–	26.7	[192]
BILP-15	Benzimidazole	448	2.61	–	–	–	63	33	[193]
BILP-16	Benzimidazole	435	2.60	–	–	–	49	32	[193]
BILP-15(AC)	Benzimidazole	862	3.41	–	–	–	50	28.9	[193]
BILP-16(AC)	Benzimidazole	643	3.41	–	–	–	49	31.6	[193]
BIPLP-1	Bis(imino)pyridine	1580	2.30	1.20	0.25	–	16	32.2	[152]
Cu/BF_4/ BIPLP-1	Bis(imino)pyridine and $CuBF_4$	380	2.5	1.75	0.53	–	64	32.3	[152]
BILP-101	Benzimidazole	536	–	2.47	0.82	71	80	33	[194]
TBILP-1	Triazine and benzimidazole	330	2.66	1.77	0.55	62	63	35	[195]
TBILP-2	Triazine and benzimidazole	1080	5.18	3.32	0.98	43	40	29	[195]
BTAP-1	Benzothiazole and sulfur chains	750	3.26	1.78	0.43	36-58	–	32	[196]
BTAP-2	Benzothiazole and sulfur chains	446	2.55	1.58	0.42	36-58	–	32	[196]
BTAP-3	Benzothiazole and sulfur chains	420	2.23	1.41	0.39	36-58	–	32	[196]
COP-19	Triazine	640	2.44	1.32	0.40	131.2			[197]
Azo-COP-1	Azo	635	2.45	1.48	0.39	63.7	–	29.3	[146]
Azo-COP-2	Azo	729	2.50	1.52	0.41	109.6	–	24.8	[146]
Azo-COP-3	Azo	493	1.91	1.18	0.36	78.6	–	32.1	[146]
TB-COP-1	Azo	1340	5.19	3.16	0.74	68.9	–	25.9	[147]
ALP-1	Azo	1235	5.36	3.25	–	28	27	29.2	[148]
ALP-2	Azo	1065	4.79	2.45	–	26	27	27.9	[148]
ALP-3	Azo	975	3.77	2.29	–	35	35	29.6	[148]

Table 2. *Continued.*

POPs	Main functional group	BET (m^2g^{-1})	CO_2 (mmol g^{-1}) 1bar, 273K	CO_2 (mmol g^{-1}) 1bar, 298K	CO_2 (mmol g^{-1}) 0.15bar, 298K	CO_2/N_2 Selectivity[a] IAST	CO_2/N_2 Selectivity[a] Henry's law	ΔH_{CO2} ($kJmol^{-1}$)	Ref.
ALP-4	Azo	862	3.52	1.84	–	26	28	28.2	[148]
ALP-6	Azo	698	3.48	2.05	0.64	–	–	28.6	[198]
ALP-7	Azo	412	2.32	1.39	0.41	–	–	30.7	[198]
POF1B	Hydroxyl	917	4.28	2.05	0.49	–	–	–	[111]
POF2B	Hydroxyl	769	3.52	1.60	0.40	–	–	–	[111]
POF3B	Hydroxyl	608	2.90	1.47	0.36	–	–	–	[111]
HAT-CTF-450/600	O-doped	1090	6.30	4.8	2.0	110	126	27.1	[199]
NPOF-1-NH_2	Aromatic amine	1535	5.84	3.77	1.07	25	–	32.1	[112]
NPOF-4-NH_2	Aromatic amine	554	2.90	1.89	–	38	40	30.1	[200]
PPN-6	None functional	4023	–	1.4	0.22[b]	–	–	17	[154]
PPN-6-SO_3H	–SO_3H	1254	–	3.6	1.15[b]	155	–	30.4	[154]
PPN-6-SO_3Li	–SO_3Li	1186	–	3.7	1.45[b]	414	–	35.7	[154]
PPN-6-SO_3NH_4	–SO_3NH_4	593	7.5	3.7	1.78[b]	–	196	40	[110]
PPN-6-CH_2Cl	Chloromethyl	1740	–	1.48	0.25[b]	13	–	21	[109]
PPN-6-DETA	Alkyl amine	555	–	4.31	3.08[b]	442	–	55	[109]
PPN-125	Hydroxyl	703	–	1.87	0.45	–	–	25	[157]
PPN-125-DETA	Alkyl amine	229	–	2.05	1.43	–	–	62	[157]
PPN-80	Alkyl amine	–	–	1.57	1.02	–	–	72	[158]
PPN-81	Alkyl amine	–	–	1.87	1.36	4716	–	54	[158]
COP-97	Melamine	59	2.34	2.09	1.52	779.2	–	46	[197]
PPN-101	Benzimidazole	1096	2.5	1.45	0.39	–	–	–	[201]
TAPOP-1	Triazine	930	4.2	–	–	–	–	27.8	[202]
TAPOP-2	Triazine	940	3.6	–	–	–	–	34.7	[202]
Fe-POP-1	Porphyrin and Fe^{3+}	875	5.21	–	–	–	–	–	[203]
Fe-POP-2	Porphyrin and Fe^{3+}	855	5.10	–	–	–	–	–	[203]
Fe-POP-3	Porphyrin and Fe^{3+}	750	2.47	–	–	–	–	–	[203]
PFPOP-1	Hydroxyl	570	3.34	1.40	0.49	43.7	–	26.9	[204]
PFPOP-2	Hydroxyl	630	4.11	1.86	0.55	52.1	–	30.2	[204]
PFPOP-3	Hydroxyl	530	4.74	2.06	0.60	56.5	–	32.5	[204]
MAPOP-1	Hydroxyl	310	2.86	1.50	0.36	–	–	29.0	[205]
MAPOP-2	Hydroxyl	660	2.77	1.55	0.43	–	–	30.6	[205]
MAPOP-3	Hydroxyl	920	2.64	1.57	0.43	–	–	31.8	[205]
MAPOP-4	Hydroxyl	820	3.07	1.80	0.45	–	–	29.5	[205]
MKPOP-1	Hydroxyl	510	1.98	1.41	0.43	–	–	23.5	[206]
MKPOP-2	Hydroxyl	160	1.43	1.07	0.39	–	–	18.3	[206]
MKPOP-3	Hydroxyl	590	2.61	1.68	0.45	–	–	27.1	[206]
MKPOP-4	Hydroxyl	480	1.93	1.32	0.43	–	–	23.6	[206]
PCP-Cl	Pyridinium, Cl^-	755	2.31	1.40	0.34	34	–	28.5	[207]
PCP-BF_4	Pyridinium, BF_4^-	586	2.20	1.33	0.34	30	–	31.6	[207]
PCP-PF_6	Pyridinium, PF_6^-	433	1.78	1.07	0.27	36	–	30.8	[207]
Polymer 1	Phosphonium	1168	2.18	1.09	0.25	–	56	35.5	[153]
Polymer 2	Phosphonium	1015	2.80	1.61	0.41	–	45	30.1	[153]
Polymer 3	Phosphonium	904	2.32	1.45	0.30	–	36	27.2	[153]
Polymer 4	Phosphonium	852	2.84	1.55	0.41	–	28	24.2	[153]

Table 2. *Continued.*

POPs	Main functional group	BET (m^2g^{-1})	CO_2 (mmol g^{-1}) 1bar, 273K	CO_2 (mmol g^{-1}) 1bar, 298K	CO_2 (mmol g^{-1}) 0.15bar, 298K	CO_2/N_2 Selectivity[a)] IAST	CO_2/N_2 Selectivity[a)] Henry's law	ΔH_{CO2} ($kJmol^{-1}$)	Ref.
Polymer 5	Phosphonium	823	2.57	1.48	0.34	–	46	25.9	[153]
Polymer 2+6	Phosphonium	770	2.93	1.70	0.45	–	–	30.1	[153]
Network A	Non-functional	4077	2.65	1.45	0.20	–	8.7	23.7	[143]
Network B	Imine	1847	3.29	1.63	0.30	–	19.5	21.8	[143]
Network C	Triazole	1237	3.86	2.20	0.5	–	14.2	33.7	[143]
Network D	Non-functional	1213	2.42	1.33	0.25	–	12.2	26.1	[143]
Network E	Non-functional	1470	2.95	1.77	0.35	–	9.2	25.4	[143]
Network F	Aromatic amine	653	1.80	1.08	0.25	–	12.2	26.7	[143]
Network G	Carbazole	1056	2.15	1.25	0.30	–	15.1	26.6	[143]
Network-1	Hydroxyl	414	1.85	1.25	–	–	16	31	[137]
Network-2	Hydroxyl	538	2.28	1.46	–	–	23	31	[137]
Network-3	Hydroxyl	333	1.89	1.24	–	–	–	31	[137]
Network-4	Hydroxyl	1015	3.96	2.27	–	–	–	31	[137]
Network-4R	Hydroxyl	927	3.46	2.21	–	–	26	31	[137]
Network-4S	Hydroxyl	981	3.50	2.21	–	–	–	31	[137]
Network-5	Hydroxyl	657	2.79	1.80	–	–	–	31	[137]
Network-6	Hydroxyl	650	2.24	1.41	–	–	–	31	[137]
CMP-1	–	837	2.05	–	–	–	–	–	[113]
CMP-1-COOH	Carboxyl group	522	1.60	–	–	–	–	–	[113]
CMP-1-$(CH_3)_2$	Methyl group	899	1.62	–	–	–	–	–	[113]
CMP-1-$(OH)_2$	Hydroxyl group	1043	1.80	–	–	–	–	–	[113]
DA-CMP-1	Aromatic amine	662	2.28	1.35	0.30	60.4	37.1	30	[114]
DA-CMP-2	Aromatic amine	603	1.64	0.95	0.24	63.1	33.1	30	[114]
TCMP-0	Triazine	963	2.38	1.34	0.25	–	9.6	–	[115]
TNCMP-2	Triazine	995	2.62	1.45	0.30	–	7.6	–	[115]
TCMP-3	Triazine	691	2.25	1.26	0.20	–	25.2	–	[115]
TCMP-5	Triazine	494	1.22	0.68	0.15	–	17.0	–	[115]
TB-MOP	Aromatic amine	694	4.05	2.57	0.80	–	50.6	–	[208]
PAF-1	Non-functional	5600	2.05	1.08	–	–	–	15.6	[145]
PAF-3	Non-functional	2932	3.48	1.82	–	–	87	19.2	[145]
PAF-4	Non-functional	2246	2.41	1.15	–	–	44	16.2	[145]
PAF-26-COOH	Carboxyl group	717	2.32	1.45	0.33	20	–	28.1	[155]
PAF-26-COOLi	Inorganic ion	591	2.54	1.61	0.36	24	–	31.8	[155]
PAF-26-COONa	Inorganic ion	483	2.67	1.61	0.36	53	–	35.0	[155]
PAF-26-COOK	Inorganic ion	430	2.41	1.54	0.40	50	–	32.6	[155]
PAF-26-COOMg	Inorganic ion	572	2.76	1.67	0.40	73	–	30.0	[155]
PAF-30	Triazine	540	2.39	1.53	0.52	–	–	36.9	[150]
PAF-33	Non-functional	821	2.16	1.25	0.27	–	19.4	27.4	[209]
PAF-33-NH_2	Amino group	370	1.19	0.75	0.33	–	79.8	32.9	[209]
PAF-33-COOH	Carboxyl group	445	1.94	1.21	0.29	–	104.3	30.0	[209]
PAF-34	Non-functional	953	2.50	1.39	0.17	–	26.3	27.2	[209]
PAF-34-OH	Hydroxyl group	771	2.21	1.25	0.27	–	39.1	30.7	[209]
PAF-35	Non-functional	567	1.77	1.01	0.22	–	29.9	30.3	[209]
PAF-56P	Triazine	553.4	–	1.52	0.33	40	–	–	[210]
POM1-IM	Imidazolium salt	926	3.16	–	–	–	–	25.6	[211]
POM2-IM	Imidazolium salt	653	3.30	–	–	13	–	31.1	[211]
POM3-IM	Imidazolium salt	575	3.23	–	–	–	–	31.5	[211]
POM4-IM	Imidazolium salt	632	2.41	–	–	–	–	–	[211]

Table 2. *Continued.*

POPs	Main functional group	BET (m^2g^{-1})	CO_2 (mmol g^{-1}) 1bar, 273K	CO_2 (mmol g^{-1}) 1bar, 298K	CO_2 (mmol g^{-1}) 0.15bar, 298K	CO_2/N_2 Selectivity[a] IAST	CO_2/N_2 Selectivity[a] Henry's law	ΔH_{CO2} ($kJmol^{-1}$)	Ref.
POM5-IM	Imidazolium salt	50	1.30	–	–	–	–	–	[211]
POM6-IM	Imidazolium salt	659	1.25	–	–	–	–	–	[211]
PON-1	Non-functional	1422	–	2.61	0.55	–	–	–	[212]
PON-2	Non-functional	168	–	0.77	0.27	–	–	–	[212]
PON-3	Non-functional	51	–	0.86	0.32	–	–	–	[212]
$[HO_2C]_{25\%}$-H_2P-COF	Carboxyl group	786	2.18	1.32	0.34	–	–	38.2	[151]
$[HO_2C]_{50\%}$-H_2P-COF	Carboxyl group	673	3.05	1.52	0.34	–	–	39.6	[151]
$[HO_2C]_{75\%}$-H_2P-COF	Carboxyl group	482	3.57	1.64	0.34	–	–	41.2	[151]
$[HO_2C]_{100\%}$-H_2P-COF	Carboxyl group	364	3.95	1.73	0.50	77	–	43.5	[151]
CPP	Triazole and amine	579	3.57	2.27	0.72	–	94	33.5	[213]
Cage 2	Imine	533	3.00	–	–	–	–	–	[214]
om-ph-MR	Melamine	256	2.50	1.77	0.86	–	100	32.2	[215]
SNU-C1-sca	Triazole	830	4.38	3.14	0.75	–	–	31.2	[216]
SNW-1	Melamine	821	–	2.19	0.67	50	–	35	[217]
TCPF-4(dried)	Aromatic amine	1404	4.66	2.86	0.80	–	56	30	[218]
TCPF-4 (humidified)	Aromatic amine	1404	3.00	1.75	–	–	–	–	[218]
TBMID	Aromatic amine	688	3.30	2.20	0.50	–	58.8	33.5	[219]
PECONF-1	Aromatic amine	499	1.86	1.34	–	135	51	29	[220]
PECONF-2	Aromatic amine	637	2.85	1.98	–	–	44	31	[220]
PECONF-3	Aromatic amine	851	3.49	2.47	–	–	41	26	[220]
PECONF-4	Aromatic amine		2.95	1.96	–	–	51	34	[220]

[a] CO_2/N_2 selectivity at 298 K. [b] CO_2 uptake at 0.15 bar and 295 K.

Several aspects of POPs have been intensively studied and applied in order to guide the design and improve the carbon-capture properties of these porous polymers. In general, it has been observed that: 1) Larger surface area will provide more adsorption sites and 2) proper design of pore sizes that are compatible with the dimensions of CO_2 molecules will significantly improve the selectivity of POPs over other gaseous components in a mixture.

3.1.1. The Effect of Surface Area on Carbon Capture

High surface area is one of the most notable properties of POPs. While high surface area may have little contribution to adsorption at low pressure,[232,238] it will dramatically increase the number of adsorption sites for CO_2 at elevated pressures, which is ideal for pre-combustion capture process.[15] At a significantly high pressure, almost all the adsorption sites on the surface are available for CO_2 binding. Additional CO_2 molecules may further condense inside the pores beyond monolayers coverages, creating multiple layers, and thus further increasing the overall capacity. It has been reported that the amount of excess CO_2 uptake is directly related to the total pore volume as well as the BET surface area.[51] PPN-4, with the highest surface area (6461 m^2 g^{-1}), showed excellent CO_2 adsorption at high pressure (3.89 mmol g^{-1} at 295 K, 50 bar).[107] Thus, targeting high-surface-area polymers is an effective method to synthesize materials with high CO_2 capacity.

Additionally, the pore properties may also affect the CO_2 capacity, which has been investigated by Jiang and co-workers.[239] The CO_2 adsorption capacities of various COF materials was simulated at high pressure (30 bar) in order to demonstrate the relationship between the CO_2 adsorption capacity and various pore properties, such as density, pore volume, BET surface area, and free volume. As shown in **Figure 3**, both the gravimetric and volumetric CO_2 capacities demonstrate corresponding trends with all four of the pore-related parameters. Specifically, the CO_2 capacity increases with surface area, porosity, and free volume, and decreases with density. As previously mentioned, at high-pressure conditions CO_2 binding is maximized, thus an adsorbent with a large free volume and surface area has more space and active sites to accommodate sorbate molecules and hence exhibit enhanced CO_2 uptake. Moreover, 3D COFs tend

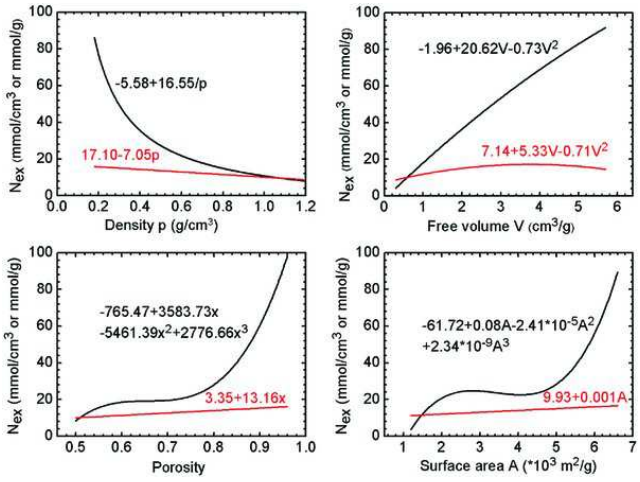

Figure 3. CO_2 capacities at 30 bar as a function of a) framework density, b) free volume, c) porosity, d) accessible surface area. Black curves: gravimetric capacity, red curves: volumetric capacity. Adapted with permission.[239] Copyright 2008, Royal Society of Chemistry.

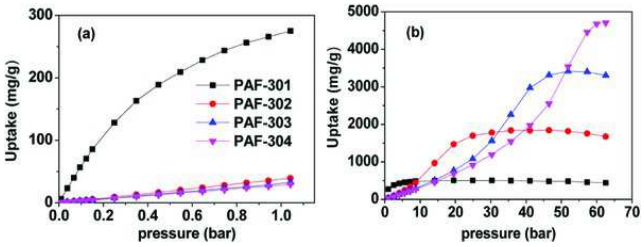

Figure 4. CO_2 adsorption isotherms at 298 K in PAFs: a) at low pressure; b) at high pressure. Reproduced with permission.[240] Copyright 2013, American Chemical Society.

to have lower density and larger free pore volume, porosity and surface area than 2D and 1D structures. As a result, 3D COFs usually have larger capacities for CO_2 adsorption at high pressures. Based on this study, the four aforementioned pore parameters could be later applied to evaluate and predict the overall theoretical saturated CO_2 capacity in other COF materials.

Theoretically, polymers formed from all-carbon–carbon bonds are expected to follow the same trend, which was evidenced by the simulated results of a series of PAF structures.[240] As shown in **Figure 4**, the CO_2 capacities of a PAF-30X series (X = 1, 2, 3, 4, representing the number of phenyl rings in the monomers) showed significant dependence on the linker length at different pressure regions. At low pressure (Figure 4a), the CO_2 adsorptions decreased in the order of PAF-301 > PAF-302 > PAF-303 > PAF-304. This order was exactly opposite to that of the linker lengths but in accord with the isosteric heats, since smaller pores lead to stronger interaction with CO_2 molecules, and isosteric heats dominate the adsorption property at lower pressure. However, structures with larger surface areas start to show higher capacities at high pressure (Figure 4b). Near the high pressure region (p > 55 bar), where CO_2 capacities are approaching the saturated values, and the condition is close to pre-combustion practice, the order of adsorption is entirely opposite to that at low pressure, i.e. PAF-304 > PAF-303 > PAF-302 > PAF-301, indicating that surface area and pore volume dominate the saturated CO_2 capacity. In contrast, Cooper et al. reported a negative correlation between surface area and linker length in a CMP series.[231] Such observations might be caused by possible network interpenetration and increased flexibility of longer linkages.

3.1.2. The Effect of Pore Size on Carbon Capture

Pore structure is one of the key properties to be studied and characterized when considering a given POP for carbon capture. In addition to the functionalities present at the pore surface, the pore size also dramatically affects the adsorption capacity and the selectivity of CO_2 over other gases. By targeting pore sizes near the kinetic diameter of CO_2 (3.3 Å), the number of double or multiple interactions between adsorbed CO_2 and the pore walls can be increased. Such strategy has been successfully used for hydrogen gas storage in different kinds of materials,[241] including COFs,[223] CMPs,[231] PIMs[242] and so on. Due to the distinct differences between the sizes and polarizabilities of CO_2 and other gas molecules,[243] tuning the pore size to around the diameter of CO_2 can lead to enhanced carbon capture performance. In such cases, CO_2 molecules can interact with multiple faces of the pores, while other gas molecules are prevented from forming strong interactions because of their lack of or reduced polarizability. Proper design of microporous structures is one key criteria to improve the selectivity by a kinetic approach.

After the first COF material was reported by Yaghi's group in 2005,[76] the pore sizes in such COFs have been well studied. As mentioned before, boroxine ring formation is reversible to some extent, resulting in polymers with some crystallinity. By applying isoreticular chemistry to COF materials, the pore sizes were enlarged symmetrically, while the relative crystalline properties were well maintained. On the other hand, carbon–carbon bond forming reactions are virtually irreversible, producing amorphous solids in most cases. For these reasons, precise control of pore properties in all-carbon–carbon-bond-containing polymers is notably difficult.

3.1.3. Polymer Sponge

Several other types of POPs have also been reported for carbon capture purposes. Among them, the hyper-cross-linked polymer (also known as "polymer sponge") reported by Cooper and coworkers is a unique candidate for pre-combustion CO_2 adsorption (**Figure 5**).[144] Similar to the carbon–carbon bonds linked polymer, this hyper-cross-linked polymer displays extraordinary stability, even in the presence of a boiling acidic solution. Although the surface area of this polymer is relatively low, the gravimetric CO_2 capacity reached 15.32 mmol g^{-1} under dry conditions at 298 K and 40 bar. The flexible nature of this polymer enables CO_2 adsorption via physical swelling, different from that of rigid materials. Performance was further enhanced at high pressures leading to a higher CO_2 capacity and an enhanced CO_2 selectivity over some of the top performing MOFs and inorganic sorbents. Moreover, the adsorption is hardly affected by the presence of water vapor due to the hydrophobicity of this

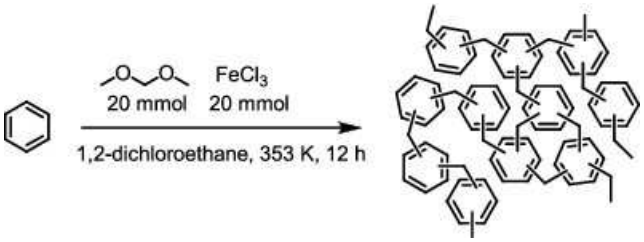

Figure 5. Synthesis of the hyper-cross-linked polymer. Adapted with permission.[144] Copyright 2014, American Chemical Society.

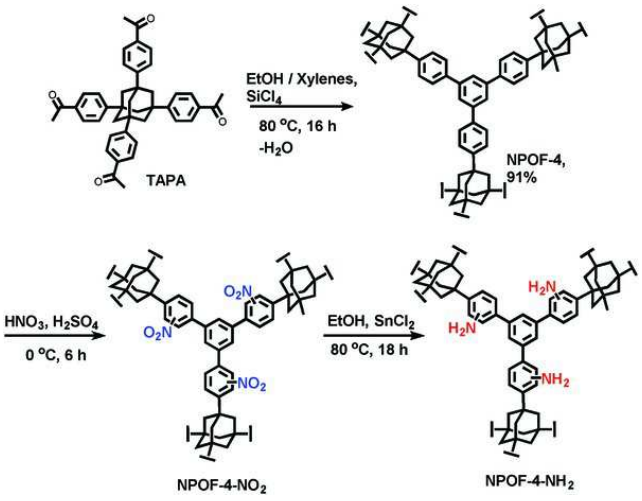

Figure 6. Schematic representation of NPOF-4 synthesis and its post-synthesis modification.

Q10

carbon-based network. The CO_2 sorption remains at 13.17 mmol g^{-1} under wet conditions at 298 K and 40 bar, which is about 86% of their dry CO_2 capacity. By contrast, the MOF sample, HKUST-1, retains only 28% of its dry CO_2 capacity under the same conditions, while zeolite 13 × only remains 6%. Its low cost, extraordinary stability, high CO_2 capacity, and excellent selectivity makes the polymer sponge a promising candidate for pre-combustion carbon capture in industrial settings.

3.2. Nitrogen-Rich Porous Organic Polymers

At this point, it is important to note that targeting high-surface-area materials may not always be the best approach to improve CO_2 capacity at low pressure. Incorporating specific functional groups in order to enhance CO_2–adsorbent interactions may be an even more effective strategy. Studies have shown that introducing nitrogen sites in POPs has great potential for increasing CO_2 uptake and selectivity of the materials through specific dipole–quadrupole interactions and/or hydrogen bonding. To date, a series of nitrogen-rich functionalities have been incorporated into POPs for higher CO_2 uptake and selectivity, including aromatic amines, imidazole, triazole, triazine, melamine, azo, imine, imide, tetrazole, and so on.

3.2.1. *Aromatic-Amine-Functionalized Porous Organic Polymers*

Aromatic-amine-based POPs refer to polymeric materials containing amine groups that are directly bound to the aromatic rings of the monomers. These POPs can be classified into three categories: primary, secondary and tertiary aromatic-amine-based materials.

In primary aromatic-amine-based POPs, the CO_2 adsorption capacities are often related to the existence of nitrogen functional sites and suitable pore sizes for CO_2.[112,114,200] For instance, by introducing $-NH_2$ groups into NPOF-4 to generate NPOF-4-NH_2, the isosteric heat of CO_2 adsorption (Q_{st}) was improved from 23.2 kJ mol^{-1} (NPOF-4) to 30.1 kJ mol^{-1} (NPOF-4-NH_2) (**Figure 6**).[200] The significant enhancement originated from the large quadrupole moment of CO_2 that forms stronger interaction with polar $-NH_2$ groups. Besides the enhanced CO_2-adsorbent affinity, post-synthetic modification produced narrower pores in NPOF-4-NH_2 than NPOF-4, that lead to higher Q_{st} in NPOF-4-NH_2 by multiple wall interactions.

Similar examples have also been reported in POPs with secondary aromatic amines, such as TBMID,[219] PECONF,[220] and PTPA-3.[244] The existence of secondary aromatic amines groups promotes favorable interactions between polymers and CO_2, thus enhancing the CO_2 uptake. There are two ways to incorporate the secondary amines into POPs. In the cases of PECONF, secondary aromatic-amine groups are introduced into the polymer via the reaction between primary amines and halogenated monomers. By removing the generated hydrogen halide, the monomers were cross-linked to form networks with a high density of secondary aromatic-amine groups. PECONF has CO_2 uptake of 3.50 mmol g^{-1} at 273 K and 1 bar. The other way to incorporate the secondary aromatic-amine groups into POPs is to employ monomers containing secondary aromatic-amine groups in polymerization, which is found in the synthesis of TBMID.[219] Following polymerization via Sonogashira–Hagihara cross-coupling, secondary aromatic-amine groups from the isoindigo monomers were successfully embodied within TBMID. As expected, the strong dipole–quadrupole interactions between secondary aromatic-amine groups and CO_2-endowed TBMID with high affinity towards CO_2, which was supported by the high isosteric heats of CO_2 adsorption (33.5 kJ mol^{-1}). TBMID also demonstrated a high CO_2 uptake of 3.30 mmol g^{-1} at 273 K and 1.13 bar with a CO_2/N_2 selectivity of 58.8.

So far, POPs containing tertiary aromatic amine groups have been reported most.[147,198,202,204,205,208,218,245] Among them, a typical example is Trger's base-derived microporous organic polymers (TB-MOPs).[208] In the synthesis of TB-MOPs, tertiary aromatic amines are formed via Trögerization of terminal amines attached to tetrahedral monomers through a one-pot metal-free synthetic approach. The CO_2 adsorption results show 4.05 mmol g^{-1} and 2.57 mmol g^{-1} at 273 K and 298 K, respectively. Besides the high CO_2 uptake, TB-MOP also exhibits excellent selectivity for CO_2 over N_2, which are 45.2 and 50.6 at 273 and 298 K, respectively. In addition, the heats of adsorption were measured in the range of 24.5–29.5 kJ mol^{-1}, which were relatively high in MOP materials but still lower than the energy of chemisorptive process. The inherent microporosity could also

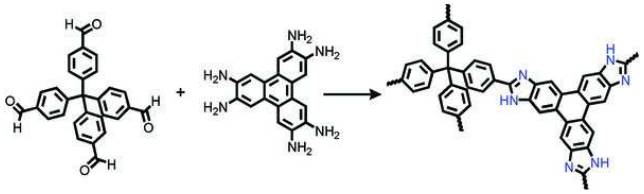

Figure 7. Synthesis of BILP-1. Reproduced with permission.[190] Copyright 2011, American Chemical Society

be responsible for the high CO_2 capacity due to multiple wall interactions.

It is worth pointing out that a general trend between the CO_2 uptake of POPs and the types of aromatic amine (primary, secondary or tertiary) cannot be concluded. The CO_2 uptake of POPs is a result of multiple variables, such as inherent pore size, surface area, and density of polar groups. In general, arylamines have less affinity towards CO_2 compared with alkylamines, since the charge density on arylamine nitrogen sites is lower than that of alkylamines. Nevertheless, arylamine incorporated POPs exhibit considerable CO_2 uptakes and could be considered as good CO_2 adsorbents with enhanced stability due to rigidity of aromatic units that promote permanent porosity.

3.2.2. Benzimidazole-Linked Organic Porous Polymers

El-Kaderi et al. reported the synthesis of a series of benzimidazole-linked polymers (BILPs) formed via condensation reactions.[149,190,191,193–195,246] For example, BILP-1, formed by the template-free synthesis from 2,3,6,7,10,11-hexaaminotriphenylene (HATP) and tetrakis(4-formylphenyl)methane (TFPM), exhibits a BET surface area of 1172 $m^2\ g^{-1}$ and CO_2 uptake of 2.97 mmol g^{-1} at 298 K and 1 bar (**Figure 7**).[190] Notably, BILP-1 is stable in the presence of 2 M HCl due to the chemical robustness of the imidazole ring. Moreover, BILP-4 shows BET surface area of 1135 $m^2\ g^{-1}$ and significantly high CO_2 uptake of 5.34 mmol g^{-1} at 273 K and 1 bar.[149] In addition, BILP-101, synthesized from 1,2,4,5-benzenetetramine tetrahydrochloride (TBA) and 1,3,5-triformylbenzene, exhibits a CO_2 uptake of 0.82 mmol g^{-1} at 298 K and 0.15 bar and exceptional CO_2 selectivity over N_2 (80) at 298 K.[194] The relatively high CO_2 uptake and selectivity over N_2 and CH_4 by BILPs are most likely because of favorable interactions of the polarizable CO_2 molecules with the framework through dipole–quadrupole interactions and/or hydrogen bonding via proton-free and protonated nitrogen sites of imidazole rings.

In order to study the effect of acid on textural properties of BILPs, HCl-free amine building units and diluted acid with variable acid/amine ratios are used in the synthesis (**Figure 8**).[193] According to the proposed mechanism of imidazole moiety formation, the acid protonates the carbonyl groups of the aldehyde moiety and catalyzes the formation of imine bond. Since imine-bond formation is reversible, acid can be used to control the rate of condensation and thus improve the surface area of the polymers. After optimizing the amount of HCl used and its concentration, the surface areas of BILP-15 and BILP-16 increased significantly by 92% and 47%. A noticable increase in CO_2 uptake was observed from 2.60 mmol g^{-1} to 3.41 mmol g^{-1} at 273 K and 1 bar.

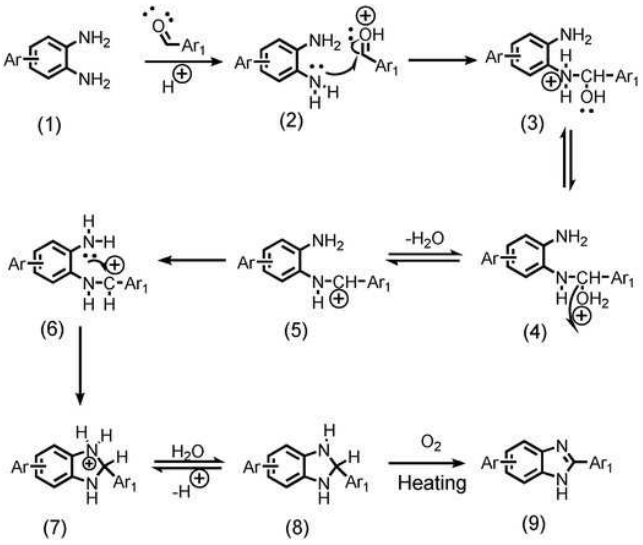

Figure 8. Proposed mechanism of imidazole moiety formation by the acid-catalyzed process. Adapted with permission.[193] Copyright 2015, American Chemical Society.

In 2014, the El-Kaderi group also reported the synthesis of triazine-based benzimidazole-linked polymers (TBILPs), namely TBILP-1 and TBILP-2, by condensation reactions of 2,4,6-tris(4-formylphenyl)-1,3,5-triazine (TFPT) with 1,2,4,5-benzenetetraamine tetrachloride (BTA) and 2,3,6,7,14,15-hexaaminotriptycene (HATT), respectively.[195] TBILP-1 shows very high selectivity (63) for CO_2 over N_2 t 298 K. TBILP-2 exhibits significantly high CO_2 uptake (5.18 mmol g^{-1}) at 1 bar and 273 K, which can be attributed to the combined effects of the Lewis basic 1,3,5-triazine and imidazole-building units of the frameworks. Both TBILPs shows the moderate isosteric heats of adsorption for CO_2, which permits high and reversible CO_2 uptake at ambient temperature. In the same year, the Zhou group reported the synthesis of PPN-101 from tetrahedral aldehyde and amine monomer.[201] PPN-101 shows a high BET surface area of 1095 $m^2\ g^{-1}$ and a CO_2 uptake of 5.34 mmol g^{-1} at 273 K and 1 bar. The calculated CO_2/N_2 selectivity is 199 due to the presence of benzimidazole units in the framework.

Pyrene-derived BILPs are also known for their high surface areas, chemical stability and N-rich pore walls, which may have a great potential in CO_2 capture and separation. Four novel pyrene-derived BILPs were synthesized by Sekizkardes and coworkers (**Figure 9**).[192] The BET surface areas of BILP-10, 11, 12, 13 were measured to be 787, 658, 1497, 677 $m^2\ g^{-1}$, respectively. Among them, BILP-12 demonstrated the highest CO_2 uptake of 5.07 mmol g^{-1} at 273 K and 1 bar, while BILP-11 had the best selectivity of 56 for CO_2/N_2 at 298 K. Overall, these BILPs are very competitive materials in terms of CO_2 capture and separation.

3.2.3. Triazole-Linked Porous Organic Polymers

Triazole-linked POPs are usually synthesized by click reactions between azide and alkynyl moieties.[216] For example, Cooper

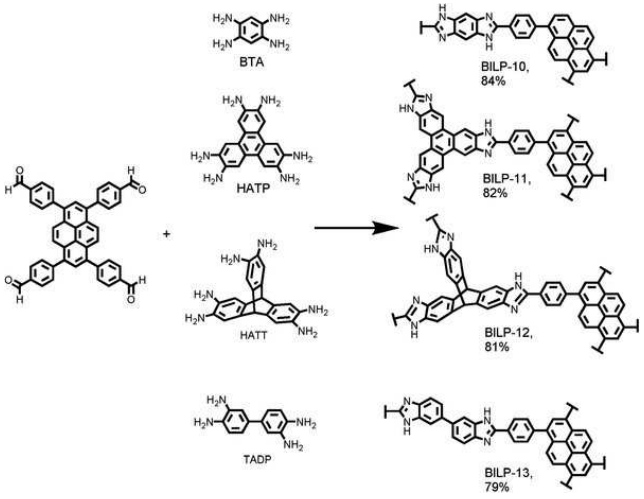

Figure 9. Synthesis of BILP-10, BILP-11, BILP-12, and BILP-13. Apated with permission.[192] Copyright 2014, Royal Society of Chemistry.

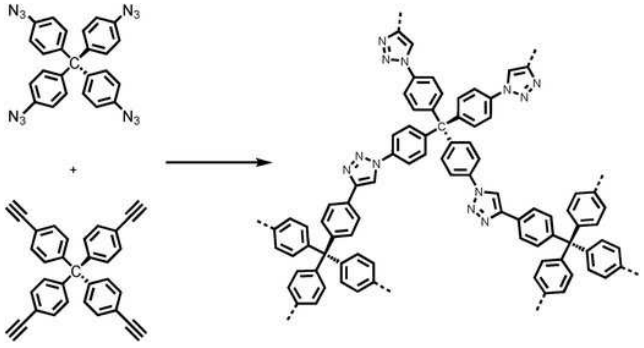

Figure 10. Synthetic route for network C. Adapted with permission.[247] Copyright 2010, American Chemical Society.

et al. reported a series of networks synthesized by click reactions (**Figure 10**).[143] Among them, network C refers to tetrahedral-based polytriazole, which is formed through click chemistry from tetrahedral monomers. Although the surface area of network C is not the highest among the studied networks, it exhibits the highest CO_2 uptake (2.20 mmol g^{-1}) at 298 K and 1 bar. The promising CO_2 uptake performance of network C most likely stems from the electron-rich triazole unit in the network. Moreover, network C has the highest heat of adsorption (33.7 kJ mol^{-1}) at low coverage compared with other networks, which is important for post-combustion carbon capture which occurs in the low pressure regime. In addition, this number is maintained at higher coverage.

3.2.4. Triazine-Linked Porous Organic Polymers

Introduction of stable electron-withdrawing triazine units into POP systems could be advantageous to both in stability and electronic structure of the POP materials.[248] Triazine-linked POPs were first developed by Thomas and co-workers through ionothermal synthesis reaction.[126] Ordered microporous POPs can be obtained from the trimerization of nitrile units in a melt

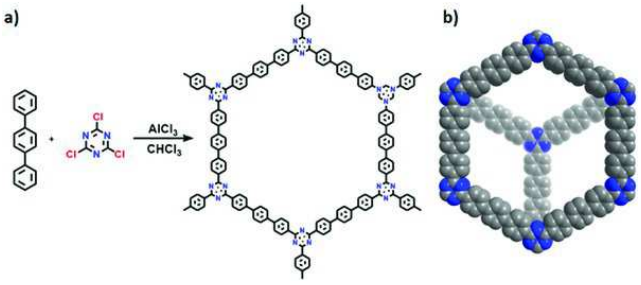

Figure 11. a) Synthesis of PAF-56P and b) PAF-56P stacked structure drawn by materials studio. Adapted with permission.[210] Copyright 2015, American Chemical Society.

$ZnCl_2$ at 400 °C. Later, perfluorinated triazine linked framework (FCTF-1) were reported by Han et al. for carbon capture.[249] The perfluorinated materials often exhibit hydrophobic and lipophobic characteristics as well as the extraordinary affinity to CO_2. In particular, FCTF-1 has the following advantages: a) the N-rich framework favors CO_2 adsorption, while the electronegativity of F can further enhance the electrostatic interactions with CO_2; b) The incorporation of F results in smaller pore size (less than 0.5 nm), which can promote the CO_2 adsorption via multiwall interactions as well as enhance CO_2-N_2 separation by kinetic selectivity; c) the hydrophobic nature of F units enables the materials great water stability, and more importantly, FCTF-1 can retain its high CO_2 capture performance even in the presence of water; d) since no strong chemical adsorption is involved, regeneration is facile.

In 2012, the Cooper group reported the synthesis of a series of conjugated microporous polymers based on electron-withdrawing 1,3,5-triazine linkage (TCMPs) by palladium-catalyzed Sonogashira–Hagihara cross-coupling reaction.[115] Although the surface areas of the TCMPs were similar to the corresponding benzene-linked CMPs, the CO_2 capacity was higher. In paticular, TNCMP-2 exhibited high surface area (995 m^2 g^{-1}) and efficient CO_2 uptake (1.45 mmol g^{-1}) at 298 K and 1 bar.

In 2015, Zhu et al. reported the synthesis of porous aromatic framework PAF-56P via cross-coupling of cyanuric chloride and *p*-terophenyl monomers (**Figure 11**).[210] PAF-56P exhibits a three dimensional framework with a large pore size of 12.0 Å and a high CO_2 uptake (1.52 mmol g^{-1}) at 298 K and 1 bar. When PAF-56P was integrated with glassy polysulfone (PSF Udel P-3500) matrices to make PAF-56P/PSF hollow fiber membranes for CO_2 capture, the membranes showed high selectivity of CO_2 over N_2 (as high as 38.9) due to the abundance of basic nitrogen sites in the PAF-56P framework.

3.2.5. Melamine-Functionalized Porous Organic Polymers

In 2014, the Zhu group reported the synthesis of N-rich SNW-1 from melamine and terephthalaldehyde monomers linked through C–N bond formation (**Figure 12**).[217] SNW-1 exhibits a three-dimensional framework with a surface area of 821 m^2 g^{-1} and major pore size around 5 Å.[250] The high CO_2 sorption capacity and selectivity of SNW-1 can be attributed to the microporous properties and existence of abundant N-H groups present within the frameworks. Small pores of SNW-1 are most likely to

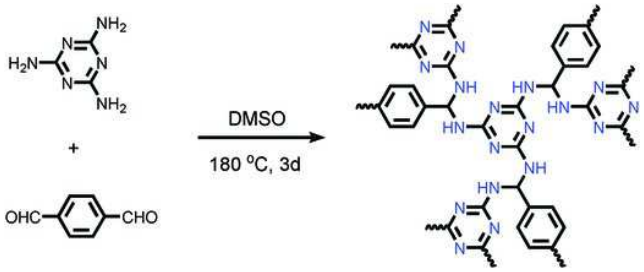

Figure 12. Schematic representation of chemical structure of SNW-1. Adapted with permission.[250] Copyright 2009 American Chemical Society.

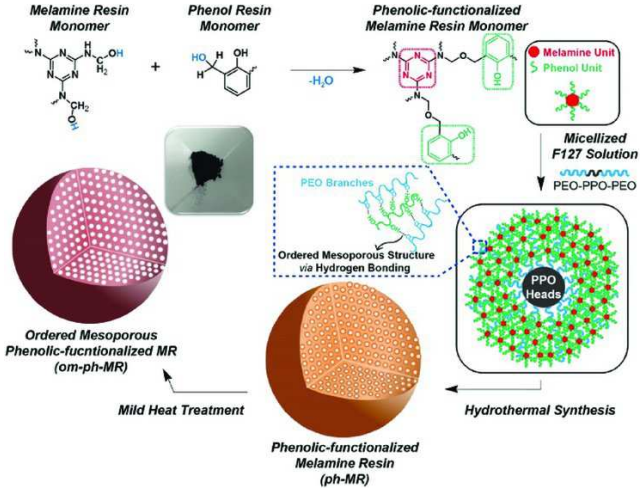

Figure 13. Schematic representation showing the synthetic route of ordered mesoporous phenolic-functionalized melamine resin (om-ph-MR). Reproduced with permission.[215] Copyright 2015, American Chemical Society.

be highly packed with CO_2 molecules via van der Waals interactions. The N–H moieties in the SNW-1 can interact strongly with CO_2 molecules, which is favorable for high CO_2 adsorption.

Despite the high N content, melamin resin (MR) cannot be used for carbon capture due to its nonporous nature. In 2015, Choi and co-workers reported a co-assembling method to make a highly-ordered mesoporous polymeric network with high nitrogen content from nonporous melamine resin monomer (**Figure 13**).[215] The phenolic resin (PR) units can form hydrogen bonding with a well known surfactant Fluroinc F127 to produce a highly ordered mesoporous copolymer network. The resultant polymer om-ph-MR shows an unexpected increased CO_2 selectivity with temperature rise. The exceptional selectivity is likely because of the abundant nitrogen moieties permitting a high binding affinity with CO_2 plus the presence of the well-defined mesopores (2.5-2.9 nm) facilitating N_2 release at higher temperature.

3.2.6. Azo-Linked Porous Organic Polymers

In 2013, Yavuz and Coskun reported the synthesis of nanoporous azo-COPs by catalyst-free coupling of aromatic nitro and amine moieties under basic conditions (**Figure 14**).[146]

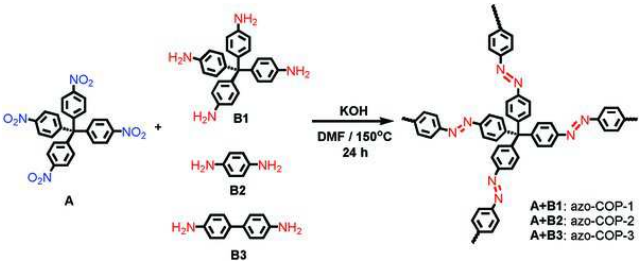

Figure 14. Synthesis route for azo-COPs. Adapted with permission.[146] Copyright 2013, rights managed by Nature Publishing Group.

Q11

These azo-COPs have BET surface areas up to 729 $m^2\ g^{-1}$ and CO_2 uptake up to 2.50 mmol g^{-1} at 273 K and 1 bar. Particularly, these azo-COPs exhibit a significant increase in the CO_2 selectivity over N_2 at increased temperature, which is most likely due to the N_2-phobic azo groups in the polymer. Monte Carlo simulations reveal that although N_2 adsorption is enthalpically favorable, the entropy loss upon binding of N_2 molecules leads to N_2 phobicity of azo groups. This work also shows the importance of azo groups in separation of CO_2 and N_2 mixtures efficiently, which is promising for post-combustion CO_2 separation. Interestingly, they went ahead and investigated four different polymerization routes for azo-COP-1, which led to completely different morphologies, surface areas, pore structures and hence the gas uptake properties.[251]

In the following year, El-Kaderi et al. reported a facile method to synthesize highly porous azo-linked polymers (ALPs) by homocoupling of aniline-like building units catalyzed by copper (I) bromide.[148] Among them, ALP-1 showes a high BET surface area of 1235 $m^2\ g^{-1}$ as well as high thermal and chemical stability. In addition, ALP-1 exhibits a remarkable gravimatrical CO_2 uptake (5.36 mmol g^{-1}) at 273 K and 1 bar. The azo group can function as the Lewis basic site, while the electron-deficient carbon atom in CO_2 can function as Lewis acid, generating enhanced dipole–quadruple interactions between these two metrics.

3.2.7. Imine-Linked Porous Organic Polymers

Utilizing the strategy of formation of imine bonds is a reversible reaction by dynamic covalent chemistry, crystalline imine-linked COFs were developed by the Yaghi group.[133] The imine-linked COFs are good candidates for carbon capture due to the enhanced affinities of nitrogen atoms to CO_2. The imine-based POPs can be synthesized by co-condensation of aldehydes with amines or hydrazides. Many research groups have focused on developing crystalline COFs via novel synthetic strategies, which would greatly promote the development of the imine linked COFs and provide better candidates for practical carbon capture.[214,252–260]

In 2012, Banerjee and co-workers reported the two imine-linked COFs, TpPa-1 and TpPa-2, for carbon capture (**Figure 15**).[261] These COFs were synthesized via Schiff base reactions of 1,3,5-triformylphloroglucinol (Tp) with p-phenylenediamine (Pa-1) and 2,5-dimethyl-p-phenylenediamine (Pa-2) under solvothermal conditions. Surprisingly, the enol-imine group un-

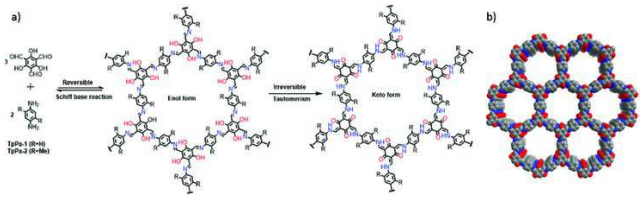

Figure 15. a) Schematic representation of the synthesis of TpPa-1 and TpPa-2 by the combined reversible and irreversible reaction of Tp with Pa-1 and Pa-2, respectively. b) TpPa-1 stacked structure drawn by materials studio.

Q12

derwent irreversible proton tautomerization to form the keto-enamine product. Both TpPa-1 and TpPa-2 showed exceptional acidic stability and water stability. TpPa-2 is stable even in 9N NaOH as TpPa-1 and TpPa-2 demonstrated reversible type-I adsorption isotherms during the N2 uptake measurement with the BET surface areas of 535 m^2 g^{-1} and 339 m^2 g^{-1}, respectively. The CO_2 adsorption of TpPa-1 and TpPa-2 are 3.48 mmol g^{-1} and 2.86 mmol g^{-1} at 273 K and 1 bar, respectively. Additionally, the synthetic strategy was applied to other starting materials, such as benzidine (BD), affording TpBD COFs. Moreover, TpBD can be obtained with solvent-free mechanochemical grinding while maintaining its crystallinity and the porosity.[262] Microwave-assisted solvothermal method was also employed to synthesize TpPa-1, which exhibited enhanced crystallinity and porosity with an increased CO_2 uptake of 4.95 mmol g^{-1} at 273 K and 1 bar.[263] To further enhance the stability and crystallinity, the Banerjee group discovered that introducing –OH units adjacent to the –C=N– centers can create intramolecular O–H···N=C hydrogen bonds.[264] The generated COF, namely DhaTph, also showed improved crystallinity and chemical stability compared with the COF lacking intramolecular hydrogen bonding. The CO_2 uptake of DhaTph is 2.91 mmol g^{-1} at 273 K and 1 bar.

An azine-linked COF, namely COF-JLU2, was designed and synthesized by condensation of 1,3,5-triformylphloroglucinol and hydrazine under solvothermal conditions (**Figure 16**).[265] COF-JLU2 combines the following merits: permanent microporosity, high crystallinity, and good stability. The BET surface area of COF-JLU2 is 410 m^2 g^{-1}, while the CO_2 uptake is 4.93 mmol g^{-1} at 273 K and 1 bar. The CO_2 adsorption capacity is comparable to some excellent POP materials, including CPOP-1 (4.81 mmol g^{-1})[266] and PPF-1 (3.09 mmol g^{-1}).[267] The excellent CO_2 capacity can be attributed to the inherent microporosity and the abundant heteroatom activated sites in the skeleton. The Q_{st} of COF-JLU2 for CO_2 was calculated to be 31 kJ mol^{-1} at low coverage. The selectivity of CO_2/N_2 was 77, which was calculated using Henry's law.

3.3. Oxygen-Rich Porous Organic Polymers

Another commonly used functional groups in POPs to enhance the CO_2 binding energy by dipole–quadrupole interactions are oxygen-containing moieties, such as the hydroxyl groups and carboxyl groups. These functional groups are highly polar, leading to the strong dipole-quadruple interactions with CO_2.

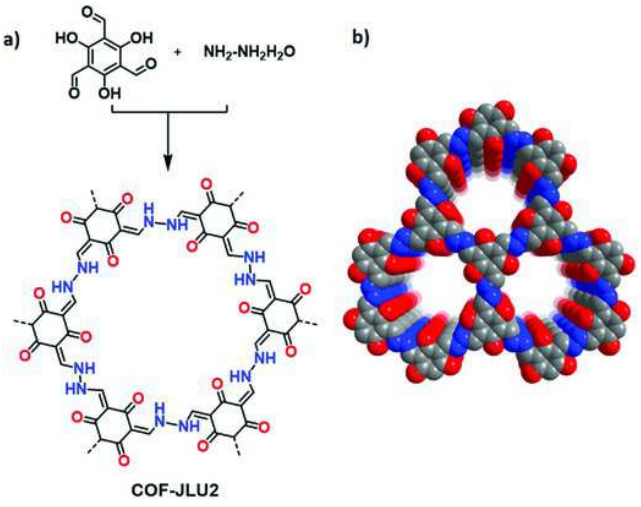

Figure 16. a) Schematic representation of the synthesis of COF-JLU2. b) Top views of the AA stacking structure of COF-JLU2.

Q13

3.3.1. Multi-Hydroxyl-Containing Porous Organic Polymers

Han's group utilized phenol formaldehyde resin (PF) chemistry to construct three hydroxyl-containing porous organic polymers (PFPOP 1–3, **Figure 17**).[204] These PFPOP materials are prepared by combining four –OH containing phenol with trialdehydes under catalyst-free conditions. Due to the carbon–carbon bond linkages, these PFPOPs demonstrate high thermal and chemical stability. All of the PFPOPs present Type I BET isotherms, with slight sorption hysteresis and the specific surface areas of PFPOP-1, PFPOP-2 and PFPOP-3 are 570, 630, and 530 m^2 g^{-1}, respectively. The microporous properties and internal structures containing abundant hydroxyl groups make these materials suitable for carbon capture. Among them, PFPOP-3 has the highest CO_2 storage capacity of 4.74 mmol g^{-1} at 273 K and 1 bar. Meanwhile, PFPOPs show considerable CO_2 over N_2 selectivity (43.7–56.5 by IAST) in the flue gas composition (CO_2/N_2 = 15/85) at 273 K and 1.0 bar. The Han group further explored this type of chemistry and created a series of mannitol-based acetal-linked POPs (MAPOPs) with decent CO_2 capacities.[205]

Compared to MAPOPs, Li and co-workers extended the aromatic acetyl monomers to more functionalities.[206] The corresponding polymers, namely mannitol-based ketal-linked porous organic polymers (MKPOPs), demonstrated BET surface areas from 160 to 590 m^2 g^{-1} with relatively low CO_2 adsorption capacities (1.43 mmol g^{-1} to 2.61 mmol g^{-1} at 273 K and 1 bar) and relative low heats of adsorption (18.3–27.1 kJ mol^{-1}).

Later, a series of alcohol-containing POPs were synthesized by Friedel–Crafts alkylation reaction of aromatic monomers and formaldehyde dimethyl acetal (FDA) (**Figure 18**).[137] CO_2 adsorptions were measured under both dry and wet conditions. For binaphthol (BINOL) network 1 & 2, naphthalen-1-ol and naphthalen-2-ol were employed as monomers, respectively. The CO_2 uptakes were found to be 1.25 mmol g^{-1} and 1.46 mmol g^{-1} at 298 K and 1 bar, respectively. For network 4, which utilized 4,4′-bi-1-naphthol, a much higher CO_2 adsorption of 2.27 mmol g^{-1} is detected at 298 K and 1 bar. At 273 K, network 4 achieved

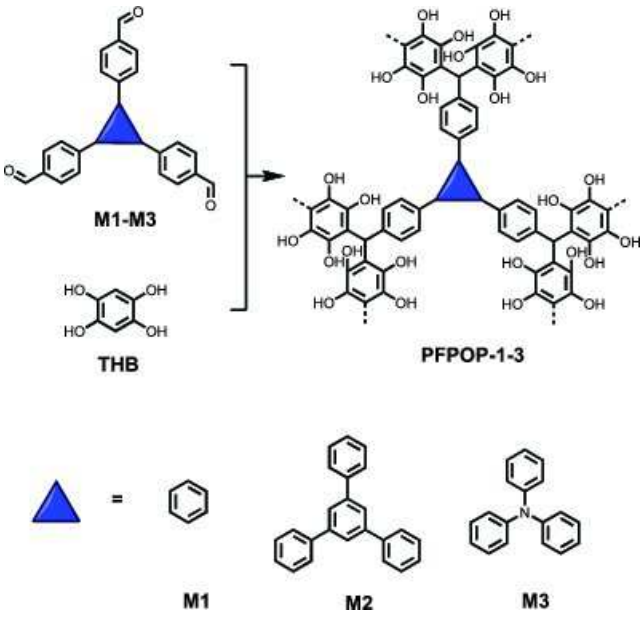

Figure 17. Synthesis of PFPOP-1, PFPOP-2, and PFPOP-3. Adapted with permission.[204] Copyright 2015, Royal Society of Chemistry.

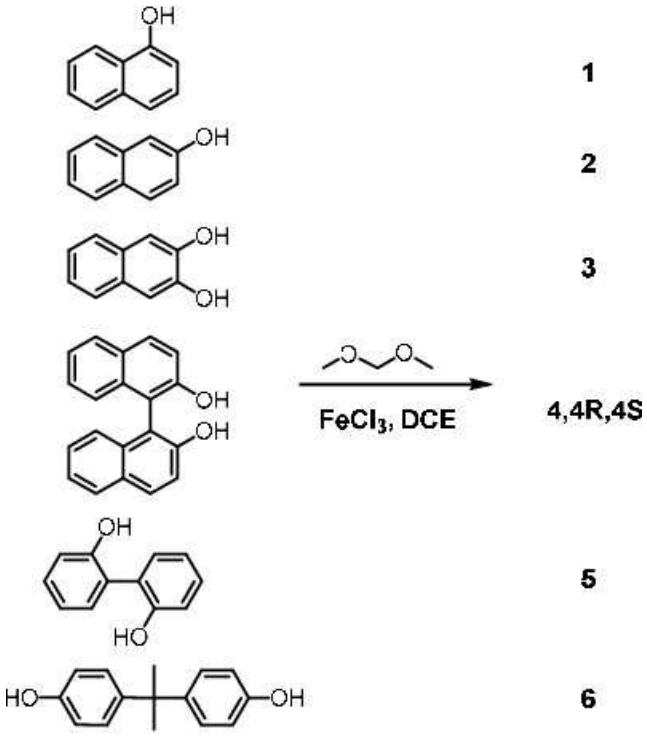

Figure 18. Synthesis of hydroxyl-containing MOP networks via Friedel–Crafts alkylation with FDA at 80 °C for 18 h. Adapted with permission.[137] Copyright 2012, American Chemical Society.

an even higher CO_2 uptake at 3.96 mmol g^{-1}. The CO_2/N_2 selectivity was calculated up to be 26 for network 4R. The authors also found that these BINOL networks, though showing high CO_2 uptake under dry conditions, actually adsorbed less CO_2 in the presence of water, indicating that high CO_2 adsorption capacities under dry condition does not guarantee high CO_2 adsorptions under more realistic wet conditions.

3.3.2. Multi-Carboxyl-Containing Porous Organic Polymers

Carboxylic acid groups have been reported to trigger a dipolar interaction with carbon dioxide.[23,57,113,268,269] Huang and coworkers successfully synthesized a series of two-dimensional COFs as outstanding CO_2 capture materials through easy channel-wall functionalization (**Figure 19**).[151] Carboxyl groups were introduced into the framework via a one step, metal-free catalytic synthesis. The carboxyl groups were located at the termini of the pore surfaces and they have similar acidity to that of the free catalytic synthesis. Those carboxyl groups were located at the terminus of the pore surfaces and they have similar acidities to that of the free carboxylic acid. Moreover, the ratio of carboxyl group was easily tuned by adjusting the amount of 2,5-dihydroxyterephthalaldehyde (DHTA) in the synthetic process. The BET surface area of $[HO_2C]_{x\%}$-H_2P-COF decreased from 786 to 364 m^2 g^{-1} after the modification, and the isosteric heat increased proportionally with the increasing amounts of carboxylic acid loading. The functionalization of channel walls with carboxylic acid groups significantly enhanced the CO_2 adsorption capacity. The CO_2 adsorption of $[HO_2C]_{100\%}$-H_2P-COF reached to 4.1 mmol g^{-1} at 273 K and 1 bar, which is one of the highest value among all the reported 2D and 3D COFs. The CO_2/N_2 selectivity of $[HO_2C]_{100\%}$-H_2P-COF was found to be 77 with the IAST methods. The CO_2 capacity of $[HO_2C]_{100\%}$-H_2P-COF was

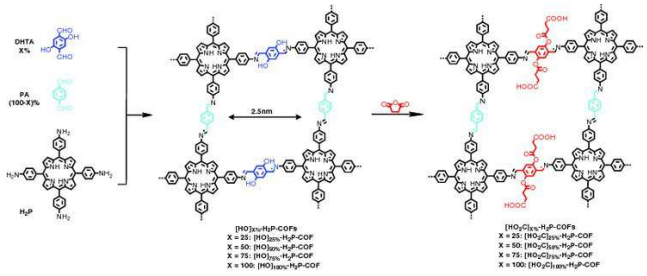

Figure 19. Synthesis of $[HO_2C]_{x\%}$-H_2P-COFs with channel walls functionalized with carboxylic acid groups through the ring opening reaction of $[OH]_{x\%}$-H_2P-COFs with succinic anhydride. Adapted with permission.[151]

also comparable to those of other top-class members.[270,271] According to the breakthrough data, the CO_2 breakthrough time for $[HO_2C]_{100\%}$-H_2P-COF (50) was much longer than that of $[HO]_{100\%}$-H_2P-COF (15). Furthermore, $[HO_2C]_{100\%}$-H_2P-COF can be recycled for more than ten cycles without significant decline in the uptake capacity, suggesting complete regeneration and excellent cycling performance.

3.3.3. O-Doped Porous Organic Polymers

The Dai group reported an in situ doping strategy to create a novel family of hexaazatriphenylene-based conjugated triazine frameworks (CTFs) displaying superior adsorption toward CO_2 at low concentrations (**Figure 20**).[199] CTFs, synthesized by the

Figure 20. Synthesis route of O-doped HAT-CTFs. Reproduced with permission.[199] Copyright 2015, American Chemical Society.

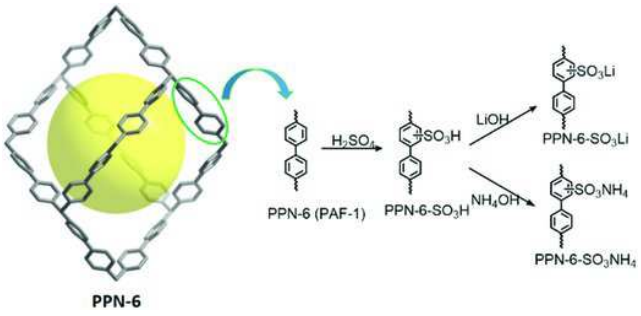

Figure 21. Synthetic route for sulfonate functionalized PPNs.

Q14

$ZnCl_2$-catalyzed high temperature technique, have extensive ultrananoporosity to provide great accessibility for CO_2 molecules to CO_2-philic sites. Interestingly, installation of methoxy groups in the starting material of CTFs would achieve in situ incorporation of O-doped active sites on the surface of the material. In addition to the intrinsic N-doped sites, these O-doped sites have significantly enhance the CO_2 affinities. The resulting material, HAT-CTF-450/600, exhibits an exceptionally high CO_2 uptake capacity (4.8 mmol g^{-1} at 297 K and 1 bar), which represents the highest CO_2 capacity under this condition. The additional O-doped sites in HAT-CTF-450/600 also affords more preferential adsorption of CO_2 over N_2.

3.4. Inorganic-Ion-Functionalized Porous Organic Polymers

Since the introduction of polar functionalities has been shown to significantly increase the isosteric heat and CO_2/N_2 adsorption selectivity,[11, 113, 268] Lu and co-workers were able to graft PPN-6 with CO_2-philic groups. PPN-6 was modified by reacting with chlorosulfonic acid to produce PPN-6-SO_3H, which was latterly neutralized to PPN-6-SO_3Li (**Figure 21**).[154] As a result of introducing functional groups into the polymer, the corresponding product PPN-6-SO_3H and PPN-6-SO_3Li demonstrated reduced BET surface areas of 1254 and 1186 m^2 g^{-1}, respectively. However, both materials have significantly increased gravimetric CO_2 uptakes with values of 3.60 mmol g^{-1} and 3.70 mmol g^{-1}, respectively. The addition of Li^+ in the framework promoted the CO_2 uptake by providing three open coordination sites to interact with CO_2 molecules electrostatically. The significant enhancement by Li^+ was also observed in the CO_2/N_2 selectivity (414 for PPN-6-SO_3Li vs. 150 for PPN-6-SO_3H) at 295 K and 1 bar. As expected, PPN-6-SO_3H and PPN-6-SO_3Li showed significantly high heats of adsorption of 30.4 and 35.7 kJ mol^{-1} at zero loading.

A later approach further extended the use of PPN-6-SO_3H by mixing with ammonia hydroxide, where the NH_4^+ moieties with reduced basicity could bind to CO_2 reversibly (Figure 21). As the result of the incorporation of NH_4^+ moieties in the network, the BET surface area further dropped to 593 m^2 g^{-1}. However, PPN-6-SO_3NH_4 demonstrated a higher CO_2 adsorption capacity (1.78 mmol g^{-1}) at 0.15 bar and 295 K, with a calculated adsorption enthalpy of 40 kJ mol^{-1} at zero-loading. This moderate heat capacity made PPN-6-SO_3NH_4 easier to regenerate compared to other top performing adsorbents. Under simulated flue gas conditions, the IAST adsorption selectivity for PPN-6-SO_3NH_4 was calculated to be 796 at 313 K and 1 bar. Moreover, the working capacity of PPN-6-SO_3NH_4 stemmed from 0.47 mmol g^{-1} between 40 °C and 120 °C, to 1.25 mmol g^{-1} between 40 °C and 150 °C.

Q15

Additionally, Ma and co-workers synthesized another series of carboxylate modified porous aromatic framework (PAF-26-COOH), followed by post-metalation with Li^+, Na^+, K^+, and Mg^{2+} for the purpose of increasing CO_2 capture.[155] After replacement of hydrogen with metal ions, the BET surface area decreased with the increasing ionic radius. However, the incorporation of metal ions led to improved CO_2 adsorption as well as the isosteric heat of adsorption. The Q_{st} of PAF-26-COOH was 28.1 kJ mol^{-1}, while that of PAF-26-COONa reached 35.0 kJ mol^{-1}. The Q_{st} values for different metal-replaced PAF-26-COOM are directly related to the basicities of their compensated alkali or alkaline earth ions. The CO_2/N_2 selectivities were measured by IAST methods, showing that all the functionalized PAF-26 materials had high selectivity.

In order to explore the influences of the ionic charge on CO_2 adsorption, Hu and co-workers used the conjugated cationic triazatriangulenium(TATA) as the skeleton to build two frameworks, TAPOP-1 and TAPOP-2.[202] Both of the polymers were synthesized via $FeCl_3$-promoted oxidative reaction of thiophene-/carbazole-functionalized TATA derivatives (**Figure 22**). TAPOP-1 and TAPOP-2 demonstrated BET specific surface areas of 930 and 940 m^2 g^{-1} with dominant microporosity. Due to the presence of charges that interact with CO_2 quadrupole moment, these two polymers exhibited relative high CO_2 uptakes with values of 4.20 mmol g^{-1} and 3.60 mmol g^{-1} at 273 K and 1 bar, respectively. The calculated heats of adsorption were 27.8 and 34.7 kJ mol^{-1}

Buyukcakir and coworkers incorporated 1,1′-bis(4-iodophenyl)-4,4′-bipyridine]-1,1′-diium salts, with counter ions Cl^-, BF_4^-, and PF_6^-, as the precursors to synthesize a series of porous cationic polymers (PCPs).[207] By increasing the ionic radius of the counter ions (PF_6^- > BF_4^- > Cl^-), the BET surface area decreased from 755 (Cl^-), 586 (BF_4^-), to 433 (PF_6^-) m^2 g^{-1}. As the introduction of counter ions into the polymers, CO_2 adsorption capacities were not improved compared to the neutral frameworks. However, the isosteric heats of adsorption were found in a range of 28.5–31.6 kJ mol^{-1}, which was much higher than the values reported for non-charged POPs with similar structures.[272] The DFT calculation indicated the binding geometries between CO_2 and pyridinium ions were

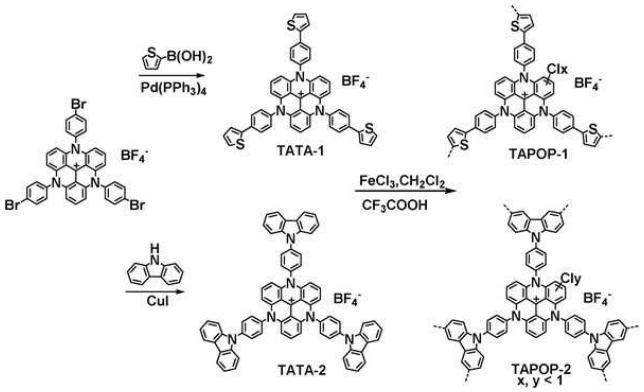

Figure 22. Synthesis of TAPOPs. Adapted with permission.[202] Copyright 2015, Royal Society of Chemistry.

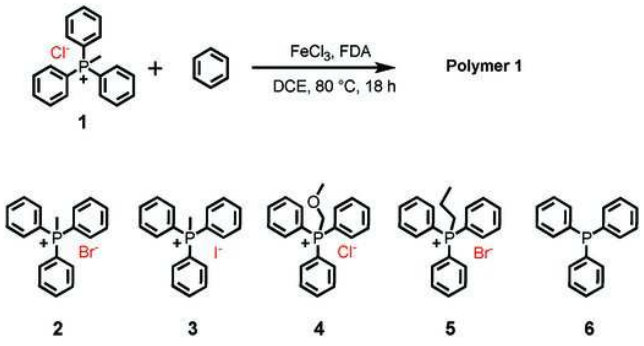

Q16 **Figure 23.** Synthesis of phosphonium–based polymers.

found similar for these three cases. Interestingly, PCP-Cl demonstrated excellent catalytic ability to convert CO_2 into cyclic carbonates due to their nucleophilicity and good leaving ability.

Considering ionic POPs could have strong interactions with CO_2, Wang and co-workers reported several hypercrosslinked phosphonium-embedded polymers (**Figure 23**).[153] The BET surface area varied from 770 to 1168 $m^2\ g^{-1}$, which could be a result of either the increasing ionic radius or increasing the length of alkyl chains. The DFT studies indicated that the phosphonium units in the polymer had high interaction energies, which was in good agreement with the high CO_2 adsorption capacity. Moreover, the CO_2/N_2 selectivity of these polymers also decreased with increasing anion size, while no significant changes resulting from the length of alkyl chains were observed. In addition, the polymer containing Br^- counter ions and methyl chain demonstrated excellent catalytic activity in the conversion of CO_2 and epoxides into cyclic carbonates, whose efficiency were much higher than the polystyrene resin-support phosphonium catalyst.

Arab and co-workers introduced the first highly porous bis(imino)pyridine linked polymer (BIPLP-1) through a bottom-up methods to generate chelating sites in the polymerization process under metal-free conditions (**Figure 24**).[152] Postsynthetic modification of BIPLP-1 was applied with $Cu(BF_4)_2$ to incorporate BF_4^- and fluorinated ions aiming at increasing the CO_2 adsorption capacity. The BET areas of the polymer were

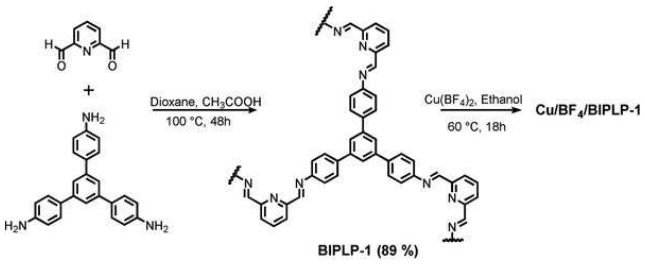

Figure 24. Synthesis of BIPLP-1 and its postsynthetic modification with $Cu(BF_4)_2$.

Q17

measured to be 1580 $m^2\ g^{-1}$ and 380 $m^2\ g^{-1}$ before and after postsynthetic modification. Though the surface areas were sacrificed for the modifications, the functionalization dramatically enhanced the CO_2 uptake capacity by 200% at 0.15 bar due to the strong CO_2-framework interactions. As a result of the postsynthetic modification, the CO_2 uptake capacity increased by 50% at 1 bar and 298 K. In addition, the CO_2/N_2 selectivity was improved from 16 to 101 at 273 K following functionalization.

Wang and co-workers successfully prepared a new series of imidazolium salt-modified porous hypercrosslinked polymer (POM-IMs) by Friedel–Crafts reaction using benzyl halides and modified with N-methylimidazole (**Figure 25**).[211] The synthetic approach is based on the one-step Friedel–Crafts alkylation between aromatic monomers and formaldehyde dimethyl acetal. Though POM-IMs' porosities decreased upon functionalization, the CO_2 uptake remained the same or increased slightly. The CO_2 capture capacity was 2.41–3.30 mmol g^{-1} at 273 K and 1 bar. These materials also demonstrated exceptional water resistance. The CO_2 capture capacities of the POP were maintained after prolonged treatment with hot water (80 °C, 18 h). Interestingly, these materials, compared to traditional polystyrene resin supported imidazolium salts and the homogeneous imidazolium salts, showed much higher activities for the conversion of CO_2 into various cyclic carbonates, which may be due to the synergistic effect of the porous structure (CO_2 capture) and the functionalized imidazolium salt (CO_2 conversion).

Porphyrin networks with high CO_2 uptake have also been reported.[273] Modak and co-workers used a facile one-pot bottom-up synthesis to achieve a series of porphyrinic Fe-POPs with exceptionally high CO_2 adsorption capacity.[203] The synthesis involved the crosslinking of repeated porphyrin units through the electrophilic substitution on pyrrole with linear di-aldehydes, phenyl complexes and small amounts of $FeCl_3$. Increasing the length of phenyl linkers, the BET surfaces areas decreased from 875, 855 to 750 $m^2\ g^{-1}$ for Fe-POP-1, -2, and -3. The strong van der Waals force between CO_2 and basic porphyrin subunits of Fe-POP-1 were most likely responsible for its high CO_2 adsorption capacity of 4.32 mmol g^{-1} at 273 K and 1 bar.

The Cu(I)-catalyzed click chemistry between alkynes and azides has been widely applied in the synthesis of polymers. Recently, a phthalocyanine-based porous polymer (CPP) was prepared via Cu(I)-catalyzed click reaction that showed a BET surface area of 579 $m^2\ g^{-1}$.[213] CPP also demonstrated very high CO_2 affinity with a value of 3.57 mmol g^{-1} (273 K) and 2.27 mmol g^{-1} (298 K) at 1 bar. In addition, the adsorption selectivity

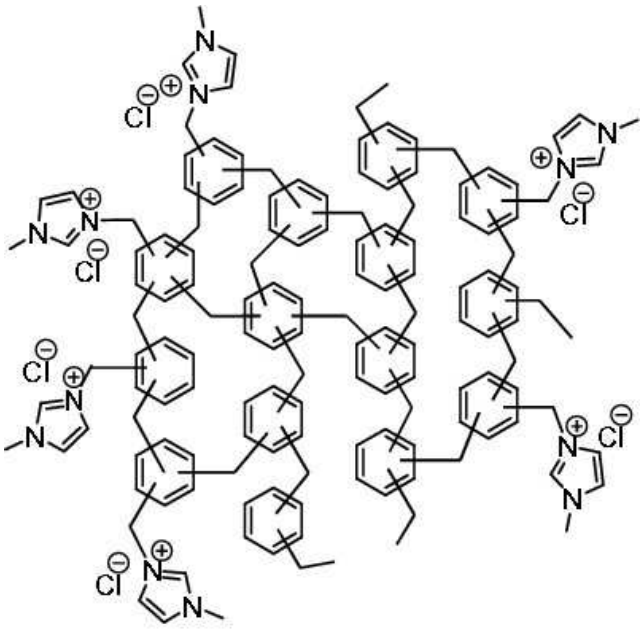

Q18 **Figure 25.** The typical structure of POM-IM.

of CPP was 94 for CO_2/N_2. The calculated heated adsorption was 33.5 kJ mol^{-1}.

3.5. Sulfur-Rich Porous Organic Polymers

Elemental sulfur is one of the most abundant elements in the world and in situ chemical impregnation of sulfur in the microporous materials can increase CO_2 affinity of the sorbent while limiting diffusion of CH_4. Recently, the Coskun group developed a solvent- and catalyst-free strategy to synthesize sulfur rich ultramicroporous benzothiazole polymers (BTAPs) in quantitative yields (**Figure 26**).[196] Elemental sulfur can be directly utilized in the synthesis of BTAPs and mediates the formation of these polymers. BTAPs were synthesized by reacting aromatic methyl monomers (M1 or M2), amine functionalized monomers (A1 or A2) and elemental sulfur (S_8) at 275 °C, followed by a heating step at 400 °C, which can remove access sulfur and activate the pores. As expected, these polymers showed excellent breakthrough CO_2 separation performance under the simulated flue gas, natural gas and landfill gas conditions. Besides, BTAPs demonstrated high regenerability values from VSA process.

3.6. Multi-Functional Porous Organic Polymers

In some cases, POPs are functionalized with several different kinds of functional groups and demonstrated very promising carbon capture properties. CMP networks were synthesized via Sonogashira–Hagihara cross-coupling reaction of 1,3,5-triethynylbenzene with either 2,5-dibromobenzoic acid or 2,5-dibromoaniline to yield the corresponding carboxylic acid- and amine-functionalized CMP networks (**Figure 27**).[113,152] Based on the BET surface data of CMPs, Dawson and co-workers concluded that the CO_2 adsorption was dependent not only on the surface area and pore volume but also the pore size and functional groups present. In terms of the functional groups, the isosteric heats of CMPs were in the order: $-COOH > -(OH)_2 > -NH_2 > -(CH_3)_2 >$ non-functionalized. This finding indicated that the acidic functional groups may surprisingly outperform aromatic-amino groups in terms of increasing CO_2 capture capacity. Compared to other reported systems, the isosteric heat of CMP-1-COOH was higher than activated carbon but lower than some MOFs, such as $HCu(Cu_4Cl)_3(BTTri)_8(en)_5$, which had high heat adsorption of 90 kJ mol^{-1}, reported by Long et al.[11]

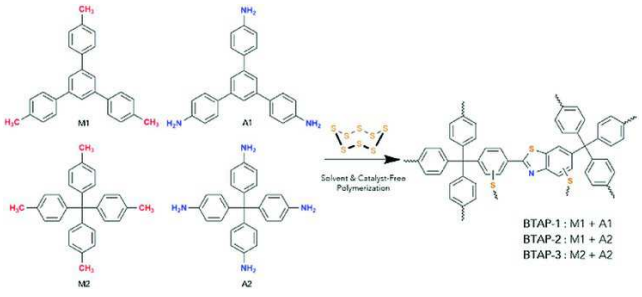

Figure 26. Synthetic scheme for the preparation of BTAPs. Reproduced with permission.[196] Copyright 2016, Elsevier Inc.

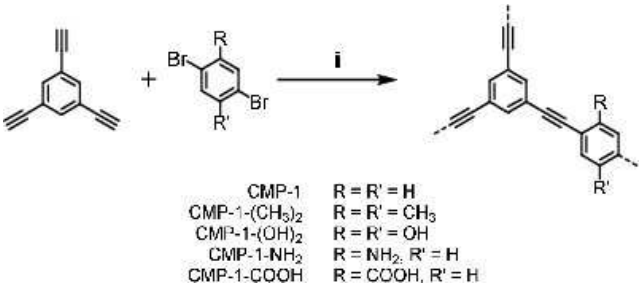

Figure 27. Synthesis of functionalized CMPs using (i) DMF, NEt_3, $Pd(PPh_3)_4$, CuI, 100°C, 72 h. Adapted with permission.[113] Copyright 2011, Royal Society of Chemistry.

A series of porous aromatic framework (PAF) materials for carbon capture were synthesized by Sonogashira–Hagihara coupling reactions using tri(4-ethynylphenyl)amine and various aryl halides.[209] Yuan and co-workers compared the unmodified PAF with –COOH, $-NH_2$, –OH functionalized PAF in terms of CO_2 adsorption capacity, isosteric heat and CO_2/N_2 selectivity. The results showed that PAF-33-COOH had the highest CO_2 uptake at 1.94 mmol g^{-1} among all the samples, which proved that the functionalization effectively improved CO_2 affinity. Based on Henry's law, these PAF materials show high CO_2 over N_2 selectivity, especially for PAF-33-NH_2 with an extraordinarily high value of 250.5, ranking PAF-33-NH_2 among the best porous adsorbents for separating CO_2 from N_2.

Different strategies have been utilized to carry out the pore surface engineering of POPs, such as quantitative click reactions between the ethynyl units and azide compounds (**Figure 28**).[171] A variety of functional groups, including ethyl, acetate, hydroxyl, carboxylic acid, and amino groups, have been tethered to the pore walls of parent COFs. The surface area, pore size and

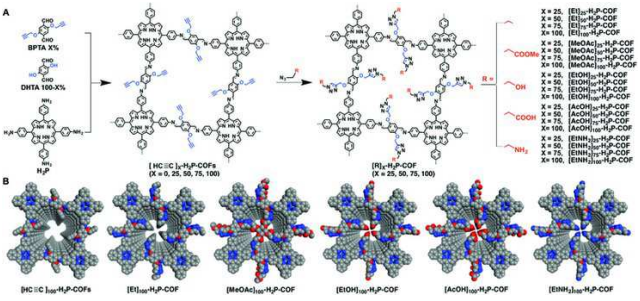

Figure 28. A) Schematic of pore surface engineering of imine-linked COFs with various functional groups via click reactions. (B) Pore structures of COFs with different functional groups (Gray, C; Blue, N; Red, O). Reproduced with permission.[171] Copyright 2015, American Chemical Society.

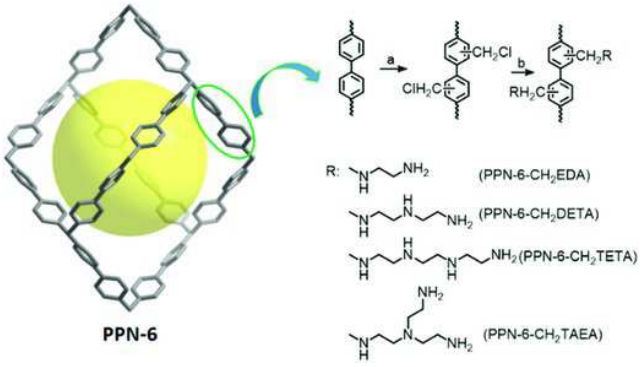

Figure 29. Synthetic route for polyamine-tethered PPNs. a: $CH_3COOH/HCl/H_3PO_4/HCHO$, 90 °C, 3 days; b: amine, 90 °C, 3 days.

Q19

pore volume decreased due to the pore surface functionalization. However, the CO_2 capacities showed to be highly dependent on the interactions of the functional groups and CO_2 molecules. The non-polar ethynyl and ethyl groups interact weekly with CO_2, resulting in poor CO_2 adsorption capacities when these functional groups were utilized. It was observed that polar ester units could interact with CO_2 via dipole–quadrupole interactions. As for carboxylic acid and the hydroxyl functionalized COFs, they interact via dipole–quadrupole and hydrogen bonding interactions, leading to enhanced CO_2 capacities. However, the amine groups, which form acid–base pairs with CO_2, led to the largest CO_2 adsorption capacity among this series of materials. To sum up, both the CO_2 capacity and heat of adsorption decreased in the order: EtNH2– > EtOH– > AcOH– > MeOAc– > Et– ≈ ethylyl–, which were in the same strength order of the interactions between functional groups and CO_2. For the strongly interacting materials, the maximal CO_2 capacities occurred when 50% of the available sites were functionalized. This observed phenomenon is the result of a balance between the two contradictory effects of enhanced affinity and decreased porosity. These results demonstrated that the precise pore surface engineering played a vital role in enhancing the CO_2 uptake.

4. Carbon Capture in Porous Organic Polymers Based on Chemical Reactions

Chemisorption of CO_2 in porous materials involves the reaction between CO_2 with functional groups in the framework. Adsorption is relatively easy in such cases due to the enthalpic favorability, but as such, also disfavors the reverse process, making regeneration a power-intensive process. Amine scrubbing process for CO_2 capture and separation has been well studies since 1930s.[274] Due to the well-understood strong interaction between amine and CO_2, capturing CO_2 by aqueous amine solution is very efficient and it is still considered as one of the record holder for CO_2 uptake. It is worth noting that the mechanisms of the reaction between CO_2 and different alkylamines are slightly different. Reactions between primary and secondary amines and CO_2 generate carbamate, whereas tertiary amines, which have steric bulky nitrogen center form bicarbonate.[275] Taking amine scrubbing as the model, aminated porous materials usually exhibit very large adsorption enthalpies for CO_2 and high CO_2/N_2 selectivity. Amine-tethered POPs are one of the most promising materials for the separation of CO_2 from other gases.[276]

In 2009, PAF-1 (also known as PPN-6), a porous polymer possessing an extremely high BET surface area of 5600m^2 g^{-1}, was synthesized via the Yamamoto–Ullman cross coupling of tetrakis(4-bromophenyl)methane.[77] Since then, several other similar porous polymers based on other tetrahedral building blocks with high surface areas were reported.[109,156,277] These polymers were functionalized with various alkylamines to increase the CO_2 uptake and the CO_2/N_2 selectivity.

Inspired by the impressive CO_2 separation results after incorporation of *N*,*N*-dimethylethylenediamine in a MOF,[278] PPN-6 was post-synthetically modified with chloromethyl groups.[109] Those chloromethyl groups were later used to tether amine groups, which selectively react with CO_2 (**Figure 29**). The modified PPN-6 demonstrated not only high CO_2 capacity but also good selectivity over nitrogen, oxygen, and other molecules commonly found in the flue gas. The best performing POP for carbon capture is PPN-6-CH_2DETA with a CO_2 uptake of 4.31 mmol g^{-1} at 1 bar and 295 K, and approximately 3.08 mmol g^{-1} at 0.15 bar and 295 K. The isosteric heat of adsorption for CO_2 is approximately 55 kJ mol^{-1}, indicating the promising nature of this material for CO_2 separation, especially at higher temperatures.

In contrast with other top performance CO_2 sorbents such as Mg-MOF-74 which collapse under moist conditions,[279] (this process has since been mitigated somewhat with MOF development to increase water stability[280]) amine-tethered POPs are not only stable to water but also have an improved CO_2 capacity, with a decent regeneration energy. Several groups have researched the mechanisms of CO_2 adsorption and put forward two possible explanations (**Figure 30**). The first mechanism suggestes that two amine moieties react with one CO_2 to produce a carbamate,[281] which can be further converted to urea with release of water and complication of later CO_2 regeneration.[282] The second mechanism involves one amine group that reacts with one CO_2 molecule and one water molecule to produce a tethered ammonium bicarbonate.

Another approach to amine tethering was demonstrated by preparing PAF-1-CH_2-phthalimide, which was then deprotected

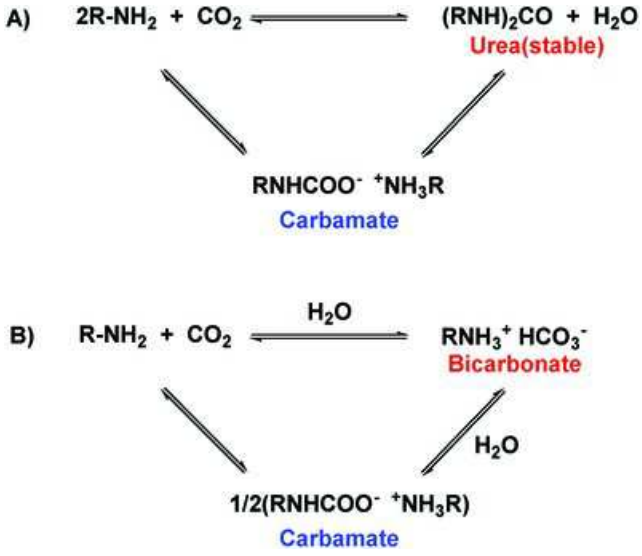

Figure 30. The mechanism of CO_2 adsorpion without moisture (A) and with moisture (B).

Q20

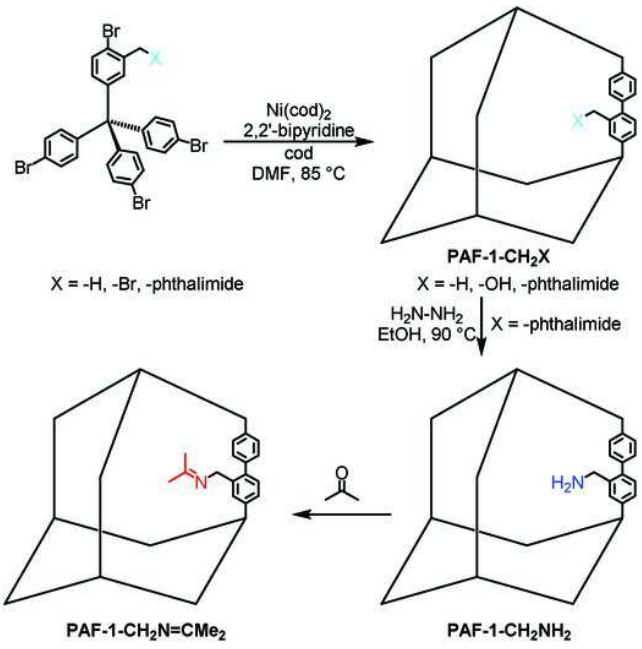

Figure 31. The synthetic procedure for the functionalized PAF-1. The PAF-1 framework is schematically represented as an adamantane cage. Adapted with permission.[277] Copyright 2012, Royal Society of Chemistry.

by hydrazine to produce PAF-1-CH_2NH_2 (**Figure 31**).[277] PAF-1-CH_2NH_2 exhibited CO_2 uptake of 4.38 mmol g^{-1} at 1 bar and 273 K and 1.52 mmol g^{-1} at 0.15 bar and 273 K. The uptake at this pressure may be analogous to the roughly 15% partial pressure of CO_2 in flue gas and thus may be a more relevant parameter for this application. Compared to the CO_2 isosteric heat of adsorption (Q_{st}) of 15.6 kJ mol^{-1} in PAF-1, the amine tetered PAF-1-CH_2NH_2 increased to 57.6 kJ mol^{-1}. As the sorption sites are filled with only one amine per anchoring site/monomer, the Q_{st} of PAF-1-CH_2NH_2 decreased quickly after initial loading.

Later investigations revealed that PPN-6-CH_2DETA had an IAST CO_2/N_2 selectivity of 3.6×10^{10} and high overall loading of 1.04 mmol g^{-1}, which are superior to other materials (**Table 3**).[156] This selectivity value can be understood better by comparing the resultant purity of gases after the mixture separation by these materials. The purity of the desorbed CO_2 from PPN-6-CH_2DETA after capture from a gas mixture of 0.04% CO_2, 78.96% N_2, and 21% O_2 is 99.999993%. The high selectivity, and the high purity of seperation, in addition to the low energy required for desorption (the heat of adsoption of 54 kJ mol^{-1}), indicate that this material is by far a top performer for direct-air capture for CO_2 and would also be ideal for other CO_2 sorbent applications such as for flue-gas capture, and especially for applications requiring maintenance of CO_2 levels in closed atmospheres such as in submarines, spacecraft, and in other scrubber and rebreather technologies.

Despite their promising performance in carbon-capure applications, amine-functionalized PAF-1/PPN-6 materials also have a major obstacle to widespread applications. Their synthesis, using Yamamoto polymerization, requires the use of an equimolar amount of bis(1,5-cyclooctadiene)nickel(0) ($Ni(COD)_2$), which is both very expensive and non-recoverable. This makes the large-scale synthesis of these materials uneconomical (though still highly promising for some applications such as in scrubbers on submarines and in space). Therefore, synthesis of POPs using other coupling reactions is necessary to lower the cost. PPN-125 (POF1B), synthesized from phloroglucinol (1,3,5-trihydroxybenzene) and terephthalaldehyde, only requires HCl as a catalyst and thus is cheap enough for widespread applications.[111,157] It also possesses exposed hydroxyl moieties which are easily functionalized with epichlorohydrin and diethylenetriamine (DETA), resulting in an extremely economical synthesis for PPN-125-DETA (**Figure 32**).

However, it has been found that a higher proportion of tetrafunctional monomers compared to bifunctional monomers was found to increase surface area in conjugated POPs, due to a greater amount of cross-linking.[285] This explains why in PPN-125, a BET surface area of only 702 $m^2 g^{-1}$ was found, as opposed to 6400 $m^2 g^{-1}$ for PPN-6.[157] After amine loading on PPN-125, a CO_2 uptake of 1.43 mmol g^{-1} was found at 298 K and 0.15 bar. The heat of adsorption for PPN-125-DETA is 61 kJ mol^{-1} at zero-coverage, and it remains high even at relatively high loadings. This high enthalpy is close to values calculated to produce adsorbents which consume a minimum amount of energy overall through temperature swing adsorption/desorption when separating CO_2 from air.[286] The high heat of adsorption also suggests a high CO_2 uptake at higher temperature. This is why POF1B, synthesized from the same reactants as PPN-125 under different conditions and investigated for CO_2 uptake with unmodified hydroxyl moieties, has very high CO_2 uptakes at 273K and atmospheric pressure, but low uptakes at 298 K and low pressure compared to amine-functionalized polymers.[111]

The low heat capacity of PPN-125-DETA leads reason to why PPN-125-DETA has a low regeneration cost that is only one-third of that of monoethanolamine aqueous solutions, which are currently used for CO_2 capture. Additionally, it was demonstrated to have over 90% capacity retention over 50 cycles of

Table 3. Comparison of CO_2 loading, IAST selectivity, and CO_2 purity data for CO_2 capture from "air" containing 400 ppm CO_2.[156]

		N_2[a]		$N_2 + O_2$[a]	
Material	CO_2 (mmol g^{-1})	S_{IAST}	Purity	S_{IAST}	Purity
MgMOF-74[283]	0.16	401	13.8	–	–
Zeolite NaX[283]	0.02	166	6.2	–	–
mmen-CuBTTri[278]	0.05	1239	33.1	–	–
PPN-6-CH_2Cl	0.001	11	0.4	11	0.4
mmen-Mg_2(dobpdc)[284]	2.05	4.9E04[b]	96.1	4.2E04[b]	94.4
PPN-6-CH_2EDA	0.15	5078	67.0	5086	67.0
PPN-6-CH_2DETA	1.04	3.8E10	99.9	3.6E10	99.9

[a] Balance gas. [b] "Molar selectivity".

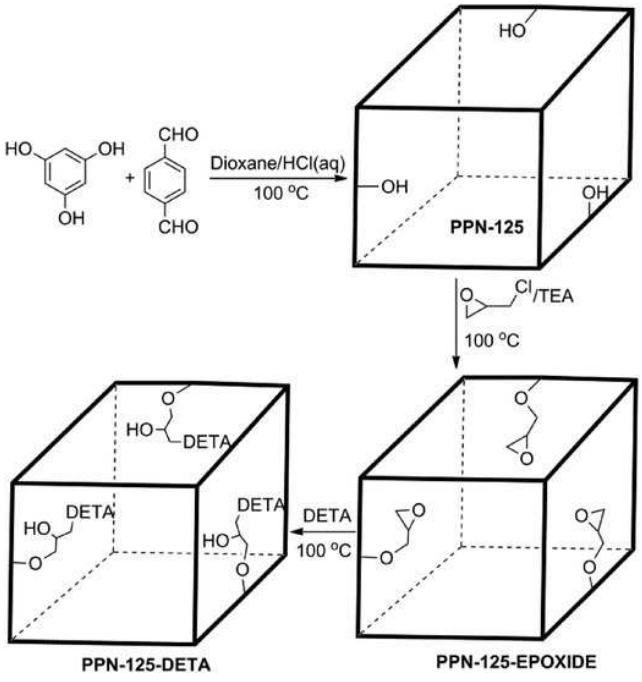

Figure 32. The synthesis of PPN-125-DETA using HCl as a polymerization catalyst, triethylamine(TEA) as a weak base to promote the reaction of the hydroxyl groups with the epichlorohydrin, and diethylenetriamine(DETA) to open the ethylene oxide ring and anchor to the polymer. Reproduced with permission.[157]

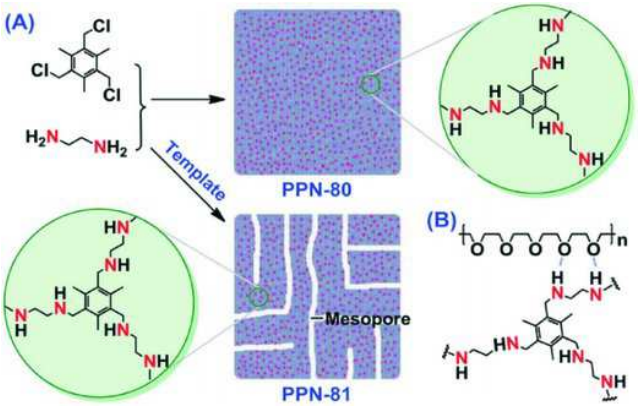

Figure 33. Polymerization of monomers to form PPN-80 in the absence of template and PPN-81 in the presence of template. Reproduced with permission.[158] Copyright 2015, Royal Society of Chemistry.

CO_2 adsorption/desorption. As all tests were conducted under dry conditions which could lead to irreversible urea formation, PPN-125-DETA should exhibit both better uptake and higher recyclability under realistic humid conditions that have yet to be tested.

Another strategy to incorporate amines into POPs was approached by using them as linkers to form a dimeric polymers. The reaction of 2,4,6-tris(chloromethyl)mesitylene and ethylene diamine produced PPN-80, while the same reaction templated with copolymer P123 produced mesoporous PPN-81 (**Figure 33**).[158] Templates have been applied to conventional polymers to enhance the porosities.[30] As for porous polymer structures, in spite of the fact that most networks guarantee the intrinsic porosities from the atomic level, using templates is also an efficient and cheap way to tune the porosities. A hiearchical system of pores was formed in PPN-81 and these mesopores not only contributed to the porosity, but also served as channels to improve the diffusion of gas molecules. At zero loading, PPN-81 had a higher heat of adsorption for CO_2 (72 kJ mol^{-1}) than that of PPN-80 (54 kJ mol^{-1}) due to the higher degree of polymerization. In other words, PPN-81 had a higher amine density than PPN-80, and acorrdingly a higher a higher CO_2 uptake at 0.15 atm (approximately 1.87 mmol g^{-1} at 295 K vs approximately 1.57 mmol g^{-1} for PPN-80). PPN-81 possessed an excellent CO_2/N_2 selectivity at 1 bar (4716), and recyclability (no loss over 6 cycles). Beased on the breakthrough experiment, the breakthrough time for CO_2 is longer than N_2 and CH_4. The adsorption temperature of 10 °C and regeneration (desorption) temperature of 60 °C tested would likely be most appropriate for applications such as in rebreathers. Overall, the relative performances between PPN-80, PPN-81, and PPN-125 suggest that a templated version of PPN-125 should be worth investigating.

PPN-6-DETA and PPN-125-DETA compare favorably to 30% MEA in all tested metrics relative to carbon-capture applications (**Table 4**). Additionally, PPN-125-DETA has both a far lower cost and higher demonstrated stability than other types of sorbent

with higher CO_2 uptakes such as mmen-CuBTTri,[278] mmen-Mg_2(dobpdc),[284] or IRMOF-74-III-CH_2NH_2,[280] MIL-101-DETA possesses similar stability and higher CO_2 uptake than PPN-125-DETA at room temperature and 0.15 atm pressure (2.13 mmol g^{-1} vs 1.43 mmol g^{-1}), but the overall cost of MIL-101-DETA synthesis is likely to be much higher.[287,288] The improvement of approximately 150% in CO_2 uptake under these conditions seen between PPN-80 and PPN-81 suggests that a templated synthesis of PPN-125 could produce a polymer with CO_2 uptake of up to 2.30 mmol g^{-1}.

Testing of these materials under realistic humid conditions may increase the total CO_2 uptake. A covalent organic polymer (COP-19) synthesized from melamine and terephthaldehyde was impregnated with polyethylamine(PEI) to make COP-97, which demonstrated a CO_2 uptake of 1.65 mmol g^{-1} at 0.15 bar and 298 K with a very high CO_2/N_2 selectivity and good recyclability over 10 cycles.[197] This uptake increased to 2.38 mmol g^{-1} when a moist mixed gas (15% CO_2, 3.8% H_2O) was used at 297 K. As the higher temperature facilitates the bicarbonate-forming reaction shown, it further increased to 2.52 mmol g^{-1} at 313 K.

In contrast, what may be currently considered one of the best solid amine CO_2 flue gas sorbents is a MOF-derived porous carbon monolith saturated with tetraethylenepentamine, TEPA@MDCM.[291] This material showed a CO_2 uptake of 5.6 mmol g^{-1} under "simulated flue gas conditions" of 75 °C (348 K) and 0.15 atm CO_2. This material demonstrates a loss of approximately 25% of its CO_2 uptake capacity over 80 adsorption/desorption cycles, and about a 12% mass loss over 90 cycles, indicating slightly less stability than a material like PPN-125-DETA with covalently tethered alkylamines. The uptake also decreased at a lower temperature, presumably due to slower adsorption kinetics in a limited adsorption time in this material with most of the pore volume saturated with amines. TEPA@MDCM may also not be low cost, due to the necessity of successively synthesizing the MOF, carbonizing it, and impregnating it with alkylamine.

In general, CO_2 uptake by solid alkylamine-based POPs under applicable conditions appears to be dominated by the density of accessible alkylamine sites. An optimal material is inexpensive, highly stable and recyclable and has an extremely high pore volume that is mostly filled with reactive alkylamines providing high uptake and selectivity.

5. Conclusion and Outlook

In conclusion, there has been significant research progress in the exploration of POPs as potential porous solid adsorbents for carbon capture. Ultrahigh-surface-area POPs can find use in the pre-combustion carbon capture, while the highly functionalized POPs can be utilized in the post-combustion carbon capture. Chemical functionalization of POPs provides abundant binding sites with CO_2 molecules, leading to higher adsorption capacities, especially at lower pressure. The affinities between POP materials and CO_2 molecules can be classified into two categories: physical interactions and chemical reactions. In the case where physical interactions dominate, bond formation is absent or negligible during the adsorption process, and thus the capacity and selectivity at low pressures will be relatively low while the regeneration process will be facile. When chemical-bond formation dominates, they usually have very high selectivity, although the regeneration takes more energy. An ideal sorbent for capturing CO_2 from post-combustion capture should have high CO_2 adsorption capacity, high selectivity, minimal regeneration energy, and long-term stability under the operating conditions.

From the foregoing discussions, it is clear that POPs are well on the way to fulfilling most of these criteria. However, there are still some aspects in urgent need of improvement: a) the crystallinity of the POPs. For the majority of the aforementioned examples, the quantity of binding sites occupied by CO_2 molecules is far less than the total calculated binding sites due to the amorphous nature of the POPs that hinders their full accessibility. For example, although a large amount of polyamines has been introduced into PPN-6-DETA through post synthetic approaches, those amine chains are not arranged in order due to the amorphous structure of PPN-6 and the flexibility of amine chains, resulting in only one-third utilization of the amine sites. Moreover, amorphous POPs are hard to characterize even by PXRD, which makes it difficult to reveal the structure of POPs and thus challenging to study the CO_2 capture mechanism. b) For now, the performance of carbon capture materials has mostly been evaluated by single-component CO_2 uptake isotherms or breakthrough experiments using a CO_2/N_2 mixed gas. However, the presence of water and other minor components (O_2, CO, SO_x, NO_x) may have significant consequences on the performances of the materials, which needs more exploration. c) The synthetic cost should be further decreased in order to scale the materials up for industrial application. The expensive catalysts, complicated monomer synthesis as well as the tedious post-functionalization would result in very high cost of the material, making it impractical for real applications. Nevertheless, tremendous efforts have already been made in improving the carbon capture properties of POP materials, and we believe that POPs are capable of serving as next-generation materials for real-world carbon capture applications.

Acknowledgements

This work was supported by the Center for Gas Separations Relevant to Clean Energy Technologies, an Energy Frontier Research Center funded by U.S. Department of Energy, Office of Science, Office of Basic Energy Sciences (DESC0001015); U.S. Department of Energy, Office of Fossil Energy, National Energy Technology Laboratory (DE-FE0026472); and the Welch Endowed Chair to HJZ (A-0030).

Conflict of Interest

The authors declare no conflict of interest.

Table 4. Calculated parameters for 30% MEA,[289,290] PPN-6-CH_2-DETA,[109,289] and PPN-125-DETA using a temperature swing adsorption/desorption carbon capture method. Values for 30% MEA and PPN-6-CH_2-DETA were taken from the literature.

Parameters	30% MEA	PPN-6-CH_2-DETA[a)]	PPN-125-DETA[b)]
Working Capacity (mmol g^{-1})	0.83	2.1	0.97
Heat capacity at 40 °C (J g^{-1} K^{-1})	3.5	1.2	1.0
Δh_{cap} (J g^{-1})	280	84	86
Δh_{ads} (J g^{-1})	100	194	48
Regeneration Energy (J g^{-1})	380	278	134
Working Capacity/Regeneration Energy (mmol kJ^{-1})	2.2	7.5	7.2
Energy Efficiency (kJ $kg^{-1}_{CO_2}$)	10 519	3019	3156

[a)] Desorption temperature is 115 °C. [b)] Desorption temperature is 120 °C

Keywords

covalent organic frameworks, porous organic polymers, porous polymer networks, post-combustion carbon capture

Received: January 11, 2017
Revised: May 2, 2017
Published Online: MM DD, YYYY

[1] M. R. Raupach, G. Marland, P. Ciais, C. Le Quéré, J. G. Canadell, G. Klepper, C. B. Field, *Proc- Natl. Acad. Sci.* **2007**, *104*, 10288.
[2] Earth System Research Laboratory, http://www.esrl.noaa.gov/gmd/ccgg/trends/index.html, accessed **2011**.
[3] R. K. Pachauri, A. Reisinger, *IPCC Fifth Assessment Report, Intergovernmental Panel on Climate Change*, **2014**.
[4] U.S. Environmental Protection Agency, http://www.epa.gov/climatechange/ccs/, accessed **June 2015**.
[5] P. Markewitz, W. Kuckshinrichs, W. Leitner, J. Linssen, P. Zapp, R. Bongartz, A. Schreiber, T. E. Muller, *Energy Environ. Sci.* **2012**, *5*, 7281.
[6] H. J. Smith, J. Fahrenkamp-Uppenbrink, R. Coontz, *Science* **2009**, *325*, 1641.
[7] M. Z. Jacobson, *Energy Environ. Sci.* **2009**, *2*, 148.
[8] D. Y. C. Leung, G. Caramanna, M. M. Maroto-Valer, *Renewable Sustainable Energy Rev.* **2014**, *39*, 426.
[9] J.-R. Li, Y. Ma, M. C. McCarthy, J. Sculley, J. Yu, H.-K. Jeong, P. B. Balbuena, H.-C. Zhou, *Coord. Chem. Rev.* **2011**, *255*, 1791.
[10] K. Sumida, D. L. Rogow, J. A. Mason, T. M. McDonald, E. D. Bloch, Z. R. Herm, T.-H. Bae, J. R. Long, *Chem. Rev.* **2012**, *112*, 724.
[11] A. Demessence, D. M. D'Alessandro, M. L. Foo, J. R. Long, *J. Am. Chem. Soc.* **2009**, *131*, 8784.
[12] S. Sircar, *Ind. Eng. Chem. Res.* **2006**, *45*, 5435.
[13] M. S. Jassim, G. T. Rochelle, *Ind. Eng. Chem. Res.* **2006**, *45*, 2465.
[14] K. B. Lee, S. Sircar, *AlChE J.* **2008**, *54*, 2293.
[15] J. D. Figueroa, T. Fout, S. Plasynski, H. McIlvried, R. D. Srivastava, *Int. J. Greenhouse Gas Control* **2008**, *2*, 9.
[16] R. Dawson, A. I. Cooper, D. J. Adams, *Polym. Int.* **2013**, *62*, 345.
[17] A. Kather, G. Scheffknecht, *Naturwissenschaften* **2009**, *96*, 993.
[18] E. Kakaras, A. Koumanakos, A. Doukelis, D. Giannakopoulos, I. Vorrias, *Fuel* **2007**, *86*, 2144.
[19] N. Passé-Coutrin, V. Jeanne-Rose, A. Ouensanga, *Fuel* **2005**, *84*, 2131.
[20] M. Tagliabue, D. Farrusseng, S. Valencia, S. Aguado, U. Ravon, C. Rizzo, A. Corma, C. Mirodatos, *Chem. Eng. J.* **2009**, *155*, 553.
[21] C.-C. Hwang, J. J. Tour, C. Kittrell, L. Espinal, L. B. Alemany, J. M. Tour, *Nat. Commun.* **2014**, *5*.
[22] A. Goeppert, M. Czaun, G. K. Surya Prakash, G. A. Olah, *Energy Environ. Sci.* **2012**, *5*, 7833.
[23] G. T. Rochelle, *Science* **2009**, *325*, 1652.
[24] Y. Zhang, B. Freeman, G. Rochelle, *Faraday Discuss.* **2016**.
[25] M. S. Walters, T. F. Edgar, G. T. Rochelle, *Ind. Eng. Chem. Res.* **2016**.
[26] A. K. Voice, *Amine Oxidation in Carbon Dioxide Capture by Aqueous Scrubbing*, **2013**.
[27] Z. Wang, W. A. Mitch, *Environ. Sci. Technol.* **2015**, *49*, 11974.
[28] B. I. Fostas, A. Gangstad, B. Nenseter, S. Pedersen, M. Sjovoll, A. L. Sorensen, *10th International Conference on Greenhouse Gas Control Technologies* **2011**, *4*, 1566.
[29] J. P. Sculley, W. M. Verdegaal, W. Lu, M. Wriedt, H. C. Zhou, *Adv. Mater.* **2013**, *25*, 3957.
[30] R. S. Haszeldine, *Science* **2009**, *325*, 1647.
[31] N. Hedin, L. Chen, A. Laaksonen, *Nanoscale* **2010**, *2*, 1819.
[32] T. C. Drage, C. E. Snape, L. A. Stevens, J. Wood, J. Wang, A. I. Cooper, R. Dawson, X. Guo, C. Satterley, R. Irons, *J. Mater. Chem.* **2012**, *22*, 2815.
[33] K. Kusakabe, T. Kuroda, A. Murata, S. Morooka, *Ind. Eng. Chem. Res.* **1997**, *36*, 649.
[34] A. N. M. Peeters, A. P. C. Faaij, W. C. Turkenburg, *Int. J. Greenhouse Gas Control* **2007**, *1*, 396.
[35] B. A. Oyenekan, G. T. Rochelle, *AlChE J.* **2007**, *53*, 3144.
[36] S. A. Freeman, R. Dugas, D. H. Van Wagener, T. Nguyen, G. T. Rochelle, *Int. J. Greenhouse Gas Control* **2010**, *4*, 119.
[37] D. M. D'Alessandro, B. Smit, J. R. Long, *Angew. Chem. Int. Ed.* **2010**, *49*, 6058.
[38] A. Samanta, A. Zhao, G. K. H. Shimizu, P. Sarkar, R. Gupta, *Ind. Eng. Chem. Res.* **2012**, *51*, 1438.
[39] Q. Wang, J. Luo, Z. Zhong, A. Borgna, *Energy Environ. Sci.* **2011**, *4*, 42.
[40] R. E. Morris, P. S. Wheatley, *Angew. Chem. Int. Ed.* **2008**, *47*, 4966.
[41] F. Akhtar, Q. Liu, N. Hedin, L. Bergstrom, *Energy Environ. Sci.* **2012**, *5*, 7664.
[42] R. V. Siriwardane, M.-S. Shen, E. P. Fisher, J. Losch, *Energy Fuels* **2005**, *19*, 1153.
[43] K. T. Chue, J. N. Kim, Y. J. Yoo, S. H. Cho, R. T. Yang, *Ind. Eng. Chem. Res.* **1995**, *34*, 591.
[44] M. O'Keeffe, M. A. Peskov, S. J. Ramsden, O. M. Yaghi, *Acc. Chem. Res.* **2008**, *41*, 1782.
[45] J. Jiang, J. Yu, A. Corma, *Angew. Chem. Int. Ed.* **2010**, *49*, 3120.

[46] S. Cavenati, C. A. Grande, A. E. Rodrigues, *Chem. Eng. Sci.* **2006**, *61*, 3893.
[47] Z. Xiang, R. Mercado, J. M. Huck, H. Wang, Z. Guo, W. Wang, D. Cao, M. Haranczyk, B. Smit, *J. Am. Chem. Soc.* **2015**, *137*, 13301.
[48] A. Phan, C. J. Doonan, F. J. Uribe-Romo, C. B. Knobler, M. O'Keeffe, O. M. Yaghi, *Acc. Chem. Res.* **2010**, *43*, 58.
[49] W. Xing, C. Liu, Z. Zhou, L. Zhang, J. Zhou, S. Zhuo, Z. Yan, H. Gao, G. Wang, S. Z. Qiao, *Energy Environ. Sci.* **2012**, *5*, 7323.
[50] A. K. Mishra, S. Ramaprabhu, *Energy Environ. Sci.* **2011**, *4*, 889.
[51] I. P. P. Cansado, M. R. Carrott, P. J. M. Carrott, *Energy Fuels* **2006**, *20*, 766.
[52] N. Hedin, L. Andersson, L. Bergström, J. Yan, *Applied Energy* **2013**, *104*, 418.
[53] M. H. Chahbani, D. Tondeur, *Sep. Purif. Technol.* **2010**, *71*, 225.
[54] J. Silvestre-Albero, A. Wahby, A. Sepulveda-Escribano, M. Martinez-Escandell, K. Kaneko, F. Rodriguez-Reinoso, *Chem. Commun.* **2011**, *47*, 6840.
[55] M. G. Plaza, S. García, F. Rubiera, J. J. Pis, C. Pevida, *Chem. Eng. J.* **2010**, *163*, 41.
[56] G. Qi, L. Fu, B. H. Choi, E. P. Giannelis, *Energy Environ. Sci.* **2012**, *5*, 7368.
[57] J. C. Hicks, J. H. Drese, D. J. Fauth, M. L. Gray, G. Qi, C. W. Jones, *J. Am. Chem. Soc.* **2008**, *130*, 2902.
[58] M. R. Mello, D. Phanon, G. Q. Silveira, P. L. Llewellyn, C. M. Ronconi, *Microporous Mesoporous Mater.* **2011**, *143*, 174.
[59] V. Zelenak, D. Halamova, L. Gaberova, E. Bloch, P. Llewellyn, *Microporous Mesoporous Mater.* **2008**, *116*, 358.
[60] S. A. Didas, S. Choi, W. Chaikittisilp, C. W. Jones, *Acc. Chem. Res.* **2015**, *48*, 2680.
[61] T. M. McDonald, W. R. Lee, J. A. Mason, B. M. Wiers, C. S. Hong, J. R. Long, *J. Am. Chem. Soc.* **2012**, *134*, 7056.
[62] S. Choi, J. H. Drese, C. W. Jones, *ChemSusChem* **2009**, *2*, 796.
[63] H. Herzog, J. Meldon, A. Hatton, *Advanced Post-Combustion CO_2 Capture*, Massachusetts Institute of Technology, Boston, MA, **2009**.
[64] J.-R. Li, R. J. Kuppler, H.-C. Zhou, *Chem. Soc. Rev.* **2009**, *38*, 1477.
[65] Y. Zeng, R. Zou, Y. Zhao, *Adv. Mater.* **2016**, *28*, 2855.
[66] X. Feng, X. Ding, D. Jiang, *Chem. Soc. Rev.* **2012**, *41*, 6010.
[67] P. Kaur, J. T. Hupp, S. T. Nguyen, *ACS Catal.* **2011**, *1*, 819.
[68] Y. Zhang, S. N. Riduan, *Chem. Soc. Rev.* **2012**, *41*, 2083.
[69] H. Furukawa, O. M. Yaghi, *J. Am. Chem. Soc.* **2009**, *131*, 8875.
[70] J. M. Simmons, H. Wu, W. Zhou, T. Yildirim, *Energy Environ. Sci.* **2011**, *4*, 2177.
[71] Y. Liu, Z. U. Wang, H.-C. Zhou, *Greenhouse Gases: Sci. Technol.* **2012**, *2*, 239.
[72] S. D. Kenarsari, D. Yang, G. Jiang, S. Zhang, J. Wang, A. G. Russell, Q. Wei, M. Fan, *RSC Adv.* **2013**, *3*, 22739.
[73] Z. Zhang, Z.-Z. Yao, S. Xiang, B. Chen, *Energy Environ. Sci.* **2014**, *7*, 2868.
[74] D. Wu, F. Xu, B. Sun, R. Fu, H. He, K. Matyjaszewski, *Chem. Rev.* **2012**, *112*, 3959.
[75] Y. Xu, S. Jin, H. Xu, A. Nagai, D. Jiang, *Chem. Soc. Rev.* **2013**, *42*, 8012.
[76] A. P. Côté, A. I. Benin, N. W. Ockwig, M. O'Keeffe, A. J. Matzger, O. M. Yaghi, *Science* **2005**, *310*, 1166.
[77] T. Ben, H. Ren, S. Ma, D. Cao, J. Lan, X. Jing, W. Wang, J. Xu, F. Deng, J. M. Simmons, S. Qiu, G. Zhu, *Angew. Chem. Int. Ed.* **2009**, *48*, 9457.
[78] S. Bandyopadhyay, P. Pallavi, A. G. Anil, A. Patra, *Polym. Chem.* **2015**, *6*, 3775.
[79] W. Lu, D. Yuan, D. Zhao, C. I. Schilling, O. Plietzsch, T. Muller, S. Bräse, J. Guenther, J. Blümel, R. Krishna, Z. Li, H.-C. Zhou, *Chem. Mater.* **2010**, *22*, 5964.
[80] H. P. Hentze, M. Antonietti, *Curr. Opin. Solid State Mater. Sci.* **2001**, *5*, 343.
[81] O. K. Farha, A. M. Spokoyny, B. G. Hauser, Y.-S. Bae, S. E. Brown, R. Q. Snurr, C. A. Mirkin, J. T. Hupp, *Chem. Mater.* **2009**, *21*, 3033.
[82] S.-Q. Xu, T.-G. Zhan, Q. Wen, Z.-F. Pang, X. Zhao, *ACS Macro Letters* **2016**, *5*, 99.
[83] V. S. Vyas, F. Haase, L. Stegbauer, G. Savasci, F. Podjaski, C. Ochsenfeld, B. V. Lotsch, *Nat. Commun.* **2015**, *6*.
[84] M. Dogru, T. Bein, *Nat Nano* **2011**, *6*, 333.
[85] C. J. Doonan, D. J. Tranchemontagne, T. G. Glover, J. R. Hunt, O. M. Yaghi, *Nat. Chem.* **2010**, *2*, 235.
[86] S. S. Han, H. Furukawa, O. M. Yaghi, W. A. Goddard, *J. Am. Chem. Soc.* **2008**, *130*, 11580.
[87] J.-T. Yu, Z. Chen, J. Sun, Z.-T. Huang, Q.-Y. Zheng, *J. Mater. Chem.* **2012**, *22*, 5369.
[88] H. Oh, S. B. Kalidindi, Y. Um, S. Bureekaew, R. Schmid, R. A. Fischer, M. Hirscher, *Angew. Chem. Int. Ed.* **2013**, *52*, 13219.
[89] H. Ma, H. Ren, S. Meng, Z. Yan, H. Zhao, F. Sun, G. Zhu, *Chem. Commun.* **2013**, *49*, 9773.
[90] S. Wan, J. Guo, J. Kim, H. Ihee, D. Jiang, *Angew. Chem. Int. Ed.* **2008**, *47*, 8826.
[91] X.-H. Liu, C.-Z. Guan, D. Wang, L.-J. Wan, *Adv. Mater.* **2014**, *26*, 6912.
[92] M. Dogru, M. Handloser, F. Auras, T. Kunz, D. Medina, A. Hartschuh, P. Knochel, T. Bein, *Angew. Chem. Int. Ed.* **2013**, *52*, 2920.
[93] M. Calik, F. Auras, L. M. Salonen, K. Bader, I. Grill, M. Handloser, D. D. Medina, M. Dogru, F. Löbermann, D. Trauner, A. Hartschuh, T. Bein, *J. Am. Chem. Soc.* **2014**, *136*, 17802.
[94] S. N. Sanders, E. Kumarasamy, A. B. Pun, M. T. Trinh, B. Choi, J. Xia, E. J. Taffet, J. Z. Low, J. R. Miller, X. Roy, X. Y. Zhu, M. L. Steigerwald, M. Y. Sfeir, L. M. Campos, *J. Am. Chem. Soc.* **2015**, *137*, 8965.
[95] S. Wan, F. Gándara, A. Asano, H. Furukawa, A. Saeki, S. K. Dey, L. Liao, M. W. Ambrogio, Y. Y. Botros, X. Duan, S. Seki, J. F. Stoddart, O. M. Yaghi, *Chem. Mater.* **2011**, *23*, 4094.
[96] Q. Fang, S. Gu, J. Zheng, Z. Zhuang, S. Qiu, Y. Yan, *Angew. Chem. Int. Ed.* **2014**, *53*, 2878.
[97] S. Lin, C. S. Diercks, Y.-B. Zhang, N. Kornienko, E. M. Nichols, Y. Zhao, A. R. Paris, D. Kim, P. Yang, O. M. Yaghi, C. J. Chang, *Science* **2015**, *349*, 1208.
[98] S.-Y. Ding, J. Gao, Q. Wang, Y. Zhang, W.-G. Song, C.-Y. Su, W. Wang, *J. Am. Chem. Soc.* **2011**, *133*, 19816.
[99] L. Stegbauer, K. Schwinghammer, B. V. Lotsch, *Chem. Sci.* **2014**, *5*, 2789.
[100] S. Chandra, T. Kundu, S. Kandambeth, R. B. Rao, Y. Marathe, S. M. Kunjir, R. Banerjee, *J. Am. Chem. Soc.* **2014**, *136*, 6570.
[101] S. Dalapati, S. Jin, J. Gao, Y. Xu, A. Nagai, D. Jiang, *J. Am. Chem. Soc.* **2013**, *135*, 17310.
[102] A. Nagai, X. Chen, X. Feng, X. Ding, Z. Guo, D. Jiang, *Angew. Chem. Int. Ed.* **2013**, *52*, 3770.
[103] G. Das, B. P. Biswal, S. Kandambeth, V. Venkatesh, G. Kaur, M. Addicoat, T. Heine, S. Verma, R. Banerjee, *Chem. Sci.* **2015**, *6*, 3931.
[104] Q. Fang, J. Wang, S. Gu, R. B. Kaspar, Z. Zhuang, J. Zheng, H. Guo, S. Qiu, Y. Yan, *J. Am. Chem. Soc.* **2015**, *137*, 8352.
[105] F. Xu, H. Xu, X. Chen, D. Wu, Y. Wu, H. Liu, C. Gu, R. Fu, D. Jiang, *Angew. Chem. Int. Ed.* **2015**, *54*, 6814.
[106] C. R. DeBlase, K. E. Silberstein, T.-T. Truong, H. D. Abruña, W. R. Dichtel, *J. Am. Chem. Soc.* **2013**, *135*, 16821.
[107] D. Yuan, W. Lu, D. Zhao, H.-C. Zhou, *Adv. Mater.* **2011**, *23*, 3723.
[108] W. Lu, M. Bosch, D. Yuan, H. C. Zhou, *ChemSusChem* **2015**, *8*, 433.

Q24

[109] W. Lu, J. P. Sculley, D. Yuan, R. Krishna, Z. Wei, H.-C. Zhou, *Angew. Chem. Int. Ed.* **2012**, *51*, 7480.
[110] W. Lu, W. M. Verdegaal, J. Yu, P. B. Balbuena, H.-K. Jeong, H.-C. Zhou, *Energy Environ. Sci.* **2013**, *6*, 3559.
[111] A. P. Katsoulidis, M. G. Kanatzidis, *Chem. Mater.* **2011**, *23*, 1818.
[112] T. Islamoglu, T. Kim, Z. Kahveci, O. M. El-Kadri, H. M. El-Kaderi, *J. Phys. Chem. C* **2016**, *120*, 2592.
[113] R. Dawson, D. J. Adams, A. I. Cooper, *Chem. Sci.* **2011**, *2*, 1173.
[114] X. Wang, Y. Zhao, L. Wei, C. Zhang, J.-X. Jiang, *J. Mater. Chem. A* **2015**, *3*, 21185.
[115] S. Ren, R. Dawson, A. Laybourn, J.-x. Jiang, Y. Khimyak, D. J. Adams, A. I. Cooper, *Polym. Chem.* **2012**, *3*, 928.
[116] N. B. McKeown, S. Makhseed, P. M. Budd, *Chem. Commun.* **2002**, 2780.
[117] N. B. McKeown, S. Hanif, K. Msayib, C. E. Tattershall, P. M. Budd, *Chem. Commun.* **2002**, 2782.
[118] N. B. McKeown, B. Gahnem, K. J. Msayib, P. M. Budd, C. E. Tattershall, K. Mahmood, S. Tan, D. Book, H. W. Langmi, A. Walton, *Angew. Chem. Int. Ed.* **2006**, *45*, 1804.
[119] P. M. Budd, A. Butler, J. Selbie, K. Mahmood, N. B. McKeown, B. Ghanem, K. Msayib, D. Book, A. Walton, *Phys. Chem. Chem. Phys.* **2007**, *9*, 1802.
[120] C. R. Mason, L. Maynard-Atem, N. M. Al-Harbi, P. M. Budd, P. Bernardo, F. Bazzarelli, G. Clarizia, J. C. Jansen, *Macromolecules* **2011**, *44*, 6471.
[121] M. G. Schwab, A. Lennert, J. Pahnke, G. Jonschker, M. Koch, I. Senkovska, M. Rehahn, S. Kaskel, *J. Mater. Chem.* **2011**, *21*, 2131.
[122] J. Germain, J. Hradil, J. M. J. Fréchet, F. Svec, *Chem. Mater.* **2006**, *18*, 4430.
[123] C. D. Wood, B. Tan, A. Trewin, H. Niu, D. Bradshaw, M. J. Rosseinsky, Y. Z. Khimyak, N. L. Campbell, R. Kirk, E. Stöckel, A. I. Cooper, *Chem. Mater.* **2007**, *19*, 2034.
[124] J.-Y. Lee, C. D. Wood, D. Bradshaw, M. J. Rosseinsky, A. I. Cooper, *Chem. Commun.* **2006**, 2670.
[125] P. Kuhn, A. Thomas, M. Antonietti, *Macromolecules* **2009**, *42*, 319.
[126] P. Kuhn, M. Antonietti, A. Thomas, *Angew. Chem. Int. Ed.* **2008**, *47*, 3450.
[127] H. Ren, T. Ben, E. Wang, X. Jing, M. Xue, B. Liu, Y. Cui, S. Qiu, G. Zhu, *Chem. Commun.* **2010**, *46*, 291.
[128] H. M. El-Kaderi, J. R. Hunt, J. L. Mendoza-Cortés, A. P. Côté, R. E. Taylor, M. O'Keeffe, O. M. Yaghi, *Science* **2007**, *316*, 268.
[129] J. R. Hunt, C. J. Doonan, J. D. LeVangie, A. P. Côté, O. M. Yaghi, *J. Am. Chem. Soc.* **2008**, *130*, 11872.
[130] E. Stockel, X. Wu, A. Trewin, C. D. Wood, R. Clowes, N. L. Campbell, J. T. A. Jones, Y. Z. Khimyak, D. J. Adams, A. I. Cooper, *Chem. Commun.* **2009**, 212.
[131] W. Frank, T. Pautzsch, E. Klemm, *Macromol. Chem. Phys.* **2001**, *202*, 2535.
[132] P. Pandey, A. P. Katsoulidis, I. Eryazici, Y. Wu, M. G. Kanatzidis, S. T. Nguyen, *Chem. Mater.* **2010**, *22*, 4974.
[133] F. J. Uribe-Romo, J. R. Hunt, H. Furukawa, C. Klöck, M. O'Keeffe, O. M. Yaghi, *J. Am. Chem. Soc.* **2009**, *131*, 4570.
[134] T.-Y. Zhou, S.-Q. Xu, Q. Wen, Z.-F. Pang, X. Zhao, *J. Am. Chem. Soc.* **2014**, *136*, 15885.
[135] S. Jin, X. Ding, X. Feng, M. Supur, K. Furukawa, S. Takahashi, M. Addicoat, M. E. El-Khouly, T. Nakamura, S. Irle, S. Fukuzumi, A. Nagai, D. Jiang, *Angew. Chem. Int. Ed.* **2013**, *52*, 2017.
[136] Y.-B. Zhang, J. Su, H. Furukawa, Y. Yun, F. Gándara, A. Duong, X. Zou, O. M. Yaghi, *J. Am. Chem. Soc.* **2013**, *135*, 16336.
[137] R. Dawson, L. A. Stevens, T. C. Drage, C. E. Snape, M. W. Smith, D. J. Adams, A. I. Cooper, *J. Am. Chem. Soc.* **2012**, *134*, 10741.
[138] R. Dawson, A. I. Cooper, D. J. Adams, *Prog. Polym. Sci.* **2012**, *37*, 530.
[139] M. Dogru, T. Bein, *Chem. Commun.* **2014**, *50*, 5531.
[140] J. W. Colson, W. R. Dichtel, *Nat. Chem.* **2013**, *5*, 453.
[141] P. J. Waller, F. Gándara, O. M. Yaghi, *Acc. Chem. Res.* **2015**, *48*, 3053.
[142] S.-Y. Ding, W. Wang, *Chem. Soc. Rev.* **2013**, *42*, 548.
[143] R. Dawson, E. Stockel, J. R. Holst, D. J. Adams, A. I. Cooper, *Energy Environ. Sci.* **2011**, *4*, 4239.
[144] R. T. Woodward, L. A. Stevens, R. Dawson, M. Vijayaraghavan, T. Hasell, I. P. Silverwood, A. V. Ewing, T. Ratvijitvech, J. D. Exley, S. Y. Chong, F. Blanc, D. J. Adams, S. G. Kazarian, C. E. Snape, T. C. Drage, A. I. Cooper, *J. Am. Chem. Soc.* **2014**, *136*, 9028.
[145] T. Ben, C. Pei, D. Zhang, J. Xu, F. Deng, X. Jing, S. Qiu, *Energy Environ. Sci.* **2011**, *4*, 3991.
[146] H. A. Patel, S. Hyun Je, J. Park, D. P. Chen, Y. Jung, C. T. Yavuz, A. Coskun, *Nat. Commun.* **2013**, *4*, 1357.
[147] J. Byun, S.-H. Je, H. A. Patel, A. Coskun, C. T. Yavuz, *J. Mater. Chem. A* **2014**, *2*, 12507.
[148] P. Arab, M. G. Rabbani, A. K. Sekizkardes, T. İslamoğlu, H. M. El-Kaderi, *Chem. Mater.* **2014**, *26*, 1385.
[149] M. G. Rabbani, H. M. El-Kaderi, *Chem. Mater.* **2012**, *24*, 1511.
[150] H. Zhao, Z. Jin, H. Su, J. Zhang, X. Yao, H. Zhao, G. Zhu, *Chem. Commun.* **2013**, *49*, 2780.
[151] N. Huang, X. Chen, R. Krishna, D. Jiang, *Angew. Chem. Int. Ed.* **2015**, *54*, 2986.
[152] P. Arab, A. Verlander, H. M. El-Kaderi, *J. Phys. Chem. C* **2015**, *119*, 8174.
[153] J. Wang, J. G. Wei Yang, G. Yi, Y. Zhang, *Chem. Commun.* **2015**, *51*, 15708.
[154] W. Lu, D. Yuan, J. Sculley, D. Zhao, R. Krishna, H.-C. Zhou, *J. Am. Chem. Soc.* **2011**, *133*, 18126.
[155] H. Ma, H. Ren, X. Zou, S. Meng, F. Sun, G. Zhu, *Polym. Chem.* **2014**, *5*, 144.
[156] W. Lu, J. P. Sculley, D. Yuan, R. Krishna, H.-C. Zhou, *J. Phys. Chem. C* **2013**, *117*, 4057.
[157] W. Lu, M. Bosch, D. Yuan, H.-C. Zhou, *ChemSusChem* **2015**, *8*, 433.
[158] L.-B. Sun, A.-G. Li, X.-D. Liu, X.-Q. Liu, D. Feng, W. Lu, D. Yuan, H.-C. Zhou, *J. Mater. Chem. A* **2015**, *3*, 3252.
[159] S. Brunauer, P. H. Emmett, E. Teller, *J. Am. Chem. Soc.* **1938**, *60*, 309.
[160] I. Langmuir, *J. Am. Chem. Soc.* **1918**, *40*, 1361.
[161] J. Weber, J. Schmidt, A. Thomas, W. Böhlmann, *Langmuir* **2010**, *26*, 15650.
[162] J. Rouquerol, P. Llewellyn, F. Rouquerol, in *Stud. Surf. Sci. Catal.*, Vol. *160* (Eds: F. R.-R. J. R. P. L. Llewellyn, N. Seaton), Elsevier, **2007**, 49.
[163] P. I. Ravikovitch, G. L. Haller, A. V. Neimark, *Adv. Colloid Interface Sci.* **1998**, *76–77*, 203.
[164] J. C. Groen, L. A. A. Peffer, J. Pérez-Ramı′rez, *Microporous Mesoporous Mater.* **2003**, *60*, 1.
[165] A. V. Neimark, Y. Lin, P. I. Ravikovitch, M. Thommes, *Carbon* **2009**, *47*, 1617.
[166] S. Yuan, W. Lu, Y.-P. Chen, Q. Zhang, T.-F. Liu, D. Feng, X. Wang, J. Qin, H.-C. Zhou, *J. Am. Chem. Soc.* **2015**, *137*, 3177.
[167] M. Eddaoudi, J. Kim, N. Rosi, D. Vodak, J. Wachter, M. O'Keeffe, O. M. Yaghi, *Science* **2002**, *295*, 469.
[168] O. K. Farha, A. Ö. Yazaydın, I. Eryazici, C. D. Malliakas, B. G. Hauser, M. G. Kanatzidis, S. T. Nguyen, R. Q. Snurr, J. T. Hupp, *Nat. Chem.* **2010**, *2*, 944.
[169] G. Lu, J. T. Hupp, *J. Am. Chem. Soc.* **2010**, *132*, 7832.
[170] S. Dalapati, E. Jin, M. Addicoat, T. Heine, D. Jiang, *J. Am. Chem. Soc.* **2016**, *138*, 5797.
[171] N. Huang, R. Krishna, D. Jiang, *J. Am. Chem. Soc.* **2015**, *137*, 7079.
[172] L. Czepirski, J. JagiełŁo, *Chem. Eng. Sci.* **1989**, *44*, 797.
[173] H. H. Pan, J. A. Ritter, P. B. Balbuena, *Langmuir* **1998**, *14*, 6323.

Q25

Q26
[174] K. Huang, Y.-T. Wu, S. Dai, *Ind. Eng. Chem. Res.* **2015**, *54*, 10126.
[175] S. Yang, X. Lin, W. Lewis, M. Suyetin, E. Bichoutskaia, J. E. Parker, C. C. Tang, D. R. Allan, P. J. Rizkallah, P. Hubberstey, N. R. Champness, K. Mark Thomas, A. J. Blake, M. Schröder, *Nat. Mater.* **2012**, *11*, 710.
[176] A. L. Myers, J. M. Prausnitz, *AlChE J.* **1965**, *11*, 121.
[177] R. Krishna, S. Calero, B. Smit, *Chem. Eng. J.* **2002**, *88*, 81.
[178] R. Krishna, J. M. van Baten, *Phys. Chem. Chem. Phys.* **2011**, *13*, 10593.
[179] B. Wang, A. P. Cote, H. Furukawa, M. O/'Keeffe, O. M. Yaghi, *Nature* **2008**, *453*, 207.
[180] P. S. Bárcia, L. Bastin, E. J. Hurtado, J. A. C. Silva, A. E. Rodrigues, B. Chen, *Sep. Sci. Technol.* **2008**, *43*, 3494.
[181] E. S. Rubin, C. Chen, A. B. Rao, *Energy Policy* **2007**, *35*, 4444.
[182] K. Z. House, C. F. Harvey, M. J. Aziz, D. P. Schrag, *Energy Environ. Sci.* **2009**, *2*, 193.
[183] Z. R. Herm, J. A. Swisher, B. Smit, R. Krishna, J. R. Long, *J. Am. Chem. Soc.* **2011**, *133*, 5664.
[184] J. Merel, M. Clausse, F. Meunier, *Ind. Eng. Chem. Res.* **2008**, *47*, 209.
[185] J. Gale, C. Hendriks, W. Turkenberg, A. H. Berger, A. S. Bhown, *Energy Procedia* **2011**, *4*, 562.
[186] T. Wang, K. S. Lackner, A. B. Wright, *Phys. Chem. Chem. Phys.* **2013**, *15*, 504.
[187] H. He, W. Li, M. Zhong, D. Konkolewicz, D. Wu, K. Yaccato, T. Rappold, G. Sugar, N. E. David, K. Matyjaszewski, *Energy Environ. Sci.* **2013**, *6*, 488.
[188] R. Ben-Mansour, M. A. Habib, O. E. Bamidele, M. Basha, N. A. A. Qasem, A. Peedikakkal, T. Laoui, M. Ali, *Appl. Energy* **2016**, *161*, 225.
[189] S. Cavenati, C. A. Grande, A. E. Rodrigues, *Energy Fuels* **2006**, *20*, 2648.
[190] M. G. Rabbani, H. M. El-Kaderi, *Chem. Mater.* **2011**, *23*, 1650.
[191] M. G. Rabbani, T. E. Reich, R. M. Kassab, K. T. Jackson, H. M. El-Kaderi, *Chem. Commun.* **2012**, *48*, 1141.
[192] A. K. Sekizkardes, T. Islamoglu, Z. Kahveci, H. M. El-Kaderi, *J. Mater. Chem. A* **2014**, *2*, 12492.
[193] S. Altarawneh, T. İslamoğlu, A. K. Sekizkardes, H. M. El-Kaderi, *Environ. Sci. Technol.* **2015**, *49*, 4715.
[194] A. K. Sekizkardes, J. T. Culp, T. Islamoglu, A. Marti, D. Hopkinson, C. Myers, H. M. El-Kaderi, H. B. Nulwala, *Chem. Commun.* **2015**, *51*, 13393.
[195] A. K. Sekizkardes, S. Altarawneh, Z. Kahveci, T. İslamoğlu, H. M. El-Kaderi, *Macromolecules* **2014**, *47*, 8328.
[196] S. H. Je, O. Buyukcakir, D. Kim, A. Coskun, *Chem* **2016**, *1*, 482.
[197] H. A. Patel, C. T. Yavuz, *Faraday Discuss.* **2015**, *183*, 401.
[198] P. Arab, E. Parrish, T. Islamoglu, H. M. El-Kaderi, *J. Mater. Chem. A* **2015**, *3*, 20586.
[199] X. Zhu, C. Tian, G. M. Veith, C. W. Abney, J. Dehaudt, S. Dai, *J. Am. Chem. Soc.* **2016**, *138*, 11497.
[200] T. Islamoglu, M. Gulam Rabbani, H. M. El-Kaderi, *J. Mater. Chem. A* **2013**, *1*, 10259.
[201] M. Zhang, Z. Perry, J. Park, H.-C. Zhou, *Polymer* **2014**, *55*, 335.
[202] X.-M. Hu, Q. Chen, Z.-Y. Sui, Z.-Q. Zhao, N. Bovet, B. W. Laursen, B.-H. Han, *RSC Adv.* **2015**, *5*, 90135.
[203] A. Modak, M. Nandi, J. Mondal, A. Bhaumik, *Chem. Commun.* **2012**, *48*, 248.
[204] S.-H. Jia, X. Ding, H.-T. Yu, B.-H. Han, *RSC Adv.* **2015**, *5*, 71095.
[205] X. Ding, H. Li, Y.-C. Zhao, B.-H. Han, *Polym. Chem.* **2015**, *6*, 5305.
[206] H. Li, X. Ding, Y.-C. Zhao, B.-H. Han, *Polymer* **2016**, *89*, 112.
[207] O. Buyukcakir, S. H. Je, D. S. Choi, S. N. Talapaneni, Y. Seo, Y. Jung, K. Polychronopoulou, A. Coskun, *Chem. Commun.* **2016**, *52*, 934.
[208] X. Zhu, C.-L. Do-Thanh, C. R. Murdock, K. M. Nelson, C. Tian, S. Brown, S. M. Mahurin, D. M. Jenkins, J. Hu, B. Zhao, H. Liu, S. Dai, *ACS Macro Lett.* **2013**, *2*, 660.
[209] R. Yuan, H. Ren, Z. Yan, A. Wang, G. Zhu, *Polym. Chem.* **2014**, *5*, 2266.
[210] L. Meng, X. Zou, S. Guo, H. Ma, Y. Zhao, G. Zhu, *ACS Appl. Mater. Interfaces* **2015**, *7*, 15561.
[211] J. Wang, W. Sng, G. Yi, Y. Zhang, *Chem. Commun.* **2015**, *51*, 12076.
[212] H. J. Jeon, J. H. Choi, Y. Lee, K. M. Choi, J. H. Park, J. K. Kang, *Adv. Energy Mater.* **2012**, *2*, 225.
[213] V. S. P. K. Neti, J. Wang, S. Deng, L. Echegoyen, *J. Mater. Chem. A* **2015**, *3*, 10284.
[214] T. Tozawa, J. T. A. Jones, S. I. Swamy, S. Jiang, D. J. Adams, S. Shakespeare, R. Clowes, D. Bradshaw, T. Hasell, S. Y. Chong, C. Tang, S. Thompson, J. Parker, A. Trewin, J. Bacsa, A. M. Z. Slawin, A. Steiner, A. I. Cooper, *Nat. Mater.* **2009**, *8*, 973.
[215] J. H. Lee, H. J. Lee, S. Y. Lim, B. G. Kim, J. W. Choi, *J. Am. Chem. Soc.* **2015**, *137*, 7210.
[216] L.-H. Xie, M. P. Suh, *Chem. Eur. J.* **2013**, *19*, 11590.
[217] X. Gao, X. Zou, H. Ma, S. Meng, G. Zhu, *Adv. Mater.* **2014**, *26*, 3644.
[218] C. Gu, D. Liu, W. Huang, J. Liu, R. Yang, *Polym. Chem.* **2015**, *6*, 7410.
[219] Y. Zhao, X. Wang, C. Zhang, F. Xie, R. Kong, J.-X. Jiang, *RSC Adv.* **2015**, *5*, 100322.
[220] P. Mohanty, L. D. Kull, K. Landskron, *Nat. Commun.* **2011**, *2*, 401.
[221] A. P. Côté, H. M. El-Kaderi, H. Furukawa, J. R. Hunt, O. M. Yaghi, *J. Am. Chem. Soc.* **2007**, *129*, 12914.
[222] M. Mastalerz, *Angew. Chem. Int. Ed.* **2008**, *47*, 445.
[223] R. W. Tilford, S. J. Mugavero, P. J. Pellechia, J. J. Lavigne, *Adv. Mater.* **2008**, *20*, 2741.
[224] D. N. Bunck, W. R. Dichtel, *Angew. Chem. Int. Ed.* **2012**, *51*, 1885.
[225] S. D. Brucks, D. N. Bunck, W. R. Dichtel, *Polymer* **2014**, *55*, 330.
[226] L. M. Lanni, R. W. Tilford, M. Bharathy, J. J. Lavigne, *J. Am. Chem. Soc.* **2011**, *133*, 13975.
[227] D. N. Bunck, W. R. Dichtel, *Chem. Commun.* **2013**, *49*, 2457.
[228] S. B. Kalidindi, C. Wiktor, A. Ramakrishnan, We, A. Schneemann, G. Van Tendeloo, R. A. Fischer, *Chem. Commun.* **2013**, *49*, 463. Q27
[229] Y. Yuan, F. Sun, H. Ren, X. Jing, W. Wang, H. Ma, H. Zhao, G. Zhu, *J. Mater. Chem.* **2011**, *21*, 13498.
[230] J.-X. Jiang, F. Su, A. Trewin, C. D. Wood, N. L. Campbell, H. Niu, C. Dickinson, A. Y. Ganin, M. J. Rosseinsky, Y. Z. Khimyak, A. I. Cooper, *Angew. Chem. Int. Ed.* **2007**, *46*, 8574.
[231] J.-X. Jiang, F. Su, A. Trewin, C. D. Wood, H. Niu, J. T. A. Jones, Y. Z. Khimyak, A. I. Cooper, *J. Am. Chem. Soc.* **2008**, *130*, 7710.
[232] R. Dawson, A. Laybourn, Y. Z. Khimyak, D. J. Adams, A. I. Cooper, *Macromolecules* **2010**, *43*, 8524.
[233] C. Zhang, Y. Liu, B. Li, B. Tan, C.-F. Chen, H.-B. Xu, X.-L. Yang, *ACS Macro Letters* **2012**, *1*, 190.
[234] W. Lu, Z. Wei, D. Yuan, J. Tian, S. Fordham, H.-C. Zhou, *Chem. Mater.* **2014**, *26*, 4589.
[235] C. D. Wood, B. Tan, A. Trewin, F. Su, M. J. Rosseinsky, D. Bradshaw, Y. Sun, L. Zhou, A. I. Cooper, *Adv. Mater.* **2008**, *20*, 1916.
[236] N. Du, H. B. Park, G. P. Robertson, M. M. Dal-Cin, T. Visser, L. Scoles, M. D. Guiver, *Nat Mater* **2011**, *10*, 372.
[237] B. G. Hauser, O. K. Farha, J. Exley, J. T. Hupp, *Chem. Mater.* **2013**, *25*, 12.
[238] C. E. Wilmer, O. K. Farha, Y.-S. Bae, J. T. Hupp, R. Q. Snurr, *Energy Environ. Sci.* **2012**, *5*, 9849.
[239] R. Babarao, J. Jiang, *Energy Environ. Sci.* **2008**, *1*, 139.
[240] Z. Yang, X. Peng, D. Cao, *J. Phys. Chem. C* **2013**, *117*, 8353.
[241] C. Weder, *Angew. Chem. Int. Ed.* **2008**, *47*, 448.

[242] B. S. Ghanem, M. Hashem, K. D. M. Harris, K. J. Msayib, M. Xu, P. M. Budd, N. Chaukura, D. Book, S. Tedds, A. Walton, N. B. McKeown, *Macromolecules* **2010**, *43*, 5287.
[243] V. Presser, J. McDonough, S.-H. Yeon, Y. Gogotsi, *Energy Environ. Sci.* **2011**, *4*, 3059.
[244] Y. Liao, J. Weber, C. F. J. Faul, *Chem. Commun.* **2014**, *50*, 8002.
[245] D. Wang, L. Li, W. Yang, Y. Zuo, S. Feng, H. Liu, *RSC Adv.* **2014**, *4*, 59877.
[246] M. G. Rabbani, A. K. Sekizkardes, O. M. El-Kadri, B. R. Kaafarani, H. M. El-Kaderi, *J. Mater. Chem.* **2012**, *22*, 25409.
[247] J. R. Holst, E. Stöckel, D. J. Adams, A. I. Cooper, *Macromolecules* **2010**, *43*, 8531.
[248] R. Gomes, P. Bhanja, A. Bhaumik, *Chem. Commun.* **2015**, *51*, 10050.
[249] Y. Zhao, K. X. Yao, B. Teng, T. Zhang, Y. Han, *Energy Environ. Sci.* **2013**, *6*, 3684.
[250] M. G. Schwab, B. Fassbender, H. W. Spiess, A. Thomas, X. Feng, K. Müllen, *J. Am. Chem. Soc.* **2009**, *131*, 7216.
[251] O. Buyukcakir, S. H. Je, J. Park, H. A. Patel, Y. Jung, C. T. Yavuz, A. Coskun, *Chem. Eur. J.* **2015**, *21*, 15320.
[252] S. Kandambeth, V. Venkatesh, D. B. Shinde, S. Kumari, A. Halder, S. Verma, R. Banerjee, *Nat. Commun.* **2015**, *6*.
[253] D. Kaleeswaran, P. Vishnoi, R. Murugavel, *J. Mater. Chem. C* **2015**, *3*, 7159.
[254] Q. Gao, L. Bai, X. Zhang, P. Wang, P. Li, Y. Zeng, R. Zou, Y. Zhao, *Chin. J. Chem.* **2015**, *33*, 90.
[255] Y. Zhu, W. Zhang, *Chem. Sci.* **2014**, *5*, 4957.
[256] M. G. Rabbani, A. K. Sekizkardes, Z. Kahveci, T. E. Reich, R. Ding, H. M. El-Kaderi, *Chem. Eur. J.* **2013**, *19*, 3324.
[257] Z. Li, X. Feng, Y. Zou, Y. Zhang, H. Xia, X. Liu, Y. Mu, *Chem. Commun.* **2014**, *50*, 13825.
[258] A. de la Peña Ruigómez, D. Rodríguez-San-Miguel, K. C. Stylianou, M. Cavallini, D. Gentili, F. Liscio, S. Milita, O. M. Roscioni , M. L. Ruiz-González, C. Carbonell, D. Maspoch, R. Mas-Ballesté, J. L. Segura, F. Zamora, *Chem. Eur. J.* **2015**, *21*, 10666.
[259] X. Yan, T. R. Cook, J. B. Pollock, P. Wei, Y. Zhang, Y. Yu, F. Huang, P. J. Stang, *J. Am. Chem. Soc.* **2014**, *136*, 4460.
[260] Y. Zeng, R. Zou, Z. Luo, H. Zhang, X. Yao, X. Ma, R. Zou, Y. Zhao, *J. Am. Chem. Soc.* **2015**, *137*, 1020.
[261] S. Kandambeth, A. Mallick, B. Lukose, M. V. Mane, T. Heine, R. Banerjee, *J. Am. Chem. Soc.* **2012**, *134*, 19524.
[262] B. P. Biswal, S. Chandra, S. Kandambeth, B. Lukose, T. Heine, R. Banerjee, *J. Am. Chem. Soc.* **2013**, *135*, 5328.
[263] H. Wei, S. Chai, N. Hu, Z. Yang, L. Wei, L. Wang, *Chem. Commun.* **2015**, *51*, 12178.
[264] S. Kandambeth, D. B. Shinde, M. K. Panda, B. Lukose, T. Heine, R. Banerjee, *Angew. Chem. Int. Ed.* **2013**, *52*, 13052.
[265] Z. Li, Y. Zhi, X. Feng, X. Ding, Y. Zou, X. Liu, Y. Mu, *Chem. Eur. J.* **2015**, *21*, 12079.
[266] Q. Chen, M. Luo, P. Hammershøj, D. Zhou, Y. Han, B. W. Laursen, C.-G. Yan, B.-H. Han, *J. Am. Chem. Soc.* **2012**, *134*, 6084.
[267] Y. Zhu, H. Long, W. Zhang, *Chem. Mater.* **2013**, *25*, 1630.
[268] A. Torrisi, R. G. Bell, C. Mellot-Draznieks, *Cryst. Growth Des.* **2010**, *10*, 2839.
[269] T. Gadzikwa, O. K. Farha, K. L. Mulfort, J. T. Hupp, S. T. Nguyen, *Chem. Commun.* **2009**, 3720.
[270] H.-L. Jiang, D. Feng, T.-F. Liu, J.-R. Li, H.-C. Zhou, *J. Am. Chem. Soc.* **2012**, *134*, 14690.
[271] L. Wang, R. T. Yang, *J. Phys. Chem. C* **2012**, *116*, 1099.
[272] Z.-Z. Yang, Y. Zhao, H. Zhang, B. Yu, Z. Ma, G. Ji, Z. Liu, *Chem. Commun.* **2014**, *50*, 13910.
[273] A. M. Shultz, O. K. Farha, J. T. Hupp, S. T. Nguyen, *Chem. Sci.* **2011**, *2*, 686.
[274] E. Blanchon le Bouhelec, P. Mougin, A. Barreau, R. Solimando, *Energy Fuels* **2007**, *21*, 2044.
[275] E. F. da Silva, H. F. Svendsen, *Int. J. Greenhouse Gas Control* **2007**, *1*, 151.
[276] B. Sreenivasulu, I. Sreedhar, P. Suresh, K. V. Raghavan, *Environ. Sci. Technol.* **2015**, *49*, 12641.
[277] S. J. Garibay, M. H. Weston, J. E. Mondloch, Y. J. Colon, O. K. Farha, J. T. Hupp, S. T. Nguyen, *CrystEngComm* **2013**, *15*, 1515.
[278] T. M. McDonald, D. M. D'Alessandro, R. Krishna, J. R. Long, *Chem. Sci.* **2011**, *2*, 2022.
[279] J. B. DeCoste, G. W. Peterson, B. J. Schindler, K. L. Killops, M. A. Browe, J. J. Mahle, *J. Mater. Chem. A* **2013**, *1*, 11922.
[280] A. M. Fracaroli, H. Furukawa, M. Suzuki, M. Dodd, S. Okajima, F. Gándara, J. A. Reimer, O. M. Yaghi, *J. Am. Chem. Soc.* **2014**, *136*, 8863.
[281] N. Planas, A. L. Dzubak, R. Poloni, L.-C. Lin, A. McManus, T. M. McDonald, J. B. Neaton, J. R. Long, B. Smit, L. Gagliardi, *J. Am. Chem. Soc.* **2013**, *135*, 7402.
[282] A. Sayari, Y. Belmabkhout, *J. Am. Chem. Soc.* **2010**, *132*, 6312.
[283] J. A. Mason, K. Sumida, Z. R. Herm, R. Krishna, J. R. Long, *Energy Environ. Sci.* **2011**, *4*, 3030.
[284] T. M. McDonald, W. R. Lee, J. A. Mason, B. M. Wiers, C. S. Hong, J. R. Long, *J. Am. Chem. Soc.* **2012**, *134*, 7056.
[285] L. J. Abbott, C. M. Colina, *J. Chem. Eng. Data* **2014**, *59*, 3177.
[286] G. D. Pirngruber, F. Guillou, A. Gomez, M. Clausse, *Int. J. Greenhouse Gas Control* **2013**, *14*, 74.
[287] Y. Lin, C. Kong, L. Chen, *RSC Adv.* **2012**, *2*, 6417.
[288] S.-N. Kim, S.-T. Yang, J. Kim, J.-E. Park, W.-S. Ahn, *CrystEngComm* **2012**, *14*, 4142.
[289] J. P. Sculley, W. M. Verdegaal, W. Lu, M. Wriedt, H.-C. Zhou, *Adv. Mater.* **2013**, *25*, 3957.
[290] R. E. Dugas, G. T. Rochelle, *Chem. Eng. Sci.* **2011**, *66*, 5212.
[291] S. Gadipelli, H. A. Patel, Z. Guo, *Adv. Mater.* **2015**, *27*, 4903.

Q1 APT to AU: please confirm that your TOC figure does not contain any elements previously published elsewhere.

Q2 APT to AU: please note that the references to manuscript sections have been removed as per journal style.

Q3 APT to AU: please provide academic titles for all authors.

Q4 APT to AU: please confirm that copyright lines are correct (note that images reproduced from other Wiley journals do not require a copyright line) and that all necessary permissions to reproduce have been received.

Q5 APT to AU: Please confirm your payment for coloured figures by sending a CCC form via email as soon as possible. This form and cost details were linked in your acceptance email. We do not publish colour online-only, so we cannot approve publication in colour without this form.

Q6 APT to AU: please check that all equations have been typeset correctly.

Q7 APT to AU: please specific which reference should be cited to match with 'Dai and co-workers.

Q8 APT to AU: please clarify mismatch between variable definition and Equation 12 (q1/qi etc).

Q9 APT to AU: please confirm that figure 2 is original and not reproduced from elsewhere.

Q10 APT to AU: please confirm that figure 6 is original and not reproduced from elsewhere.

Q11 APT to AU: please clarify, who holds the copyright for figure 14?

Q12 APT to AU: please confirm that figure 15 is original and not reproduced from elsewhere

Q13 APT to AU: please confirm that figure 16 is original and not reproduced from elsewhere.

Q14 APT to AU: please confirm that figure 21 is original and not reproduced from elsewhere.

Q15 APT to AU: please check changes to previous sentence.

Q16 APT to AU: please confirm that figure 23 is original and not reproduced from elsewhere.

Q17 APT to AU: please confirm that figure 24 is original and not reproduced from elsewhere.

Q18 APT to AU: please confirm that figure 25 is original and not reproduced from elsewhere.

Q19 APT to AU: please confirm that figure 29 is original and not reproduced from elsewhere.

Q20 APT to AU: please confirm that figure 30 is original and not reproduced from elsewhere

Q21 APT to AU: please give month and year reference 2 was most recently accessed.

Q22 APT to AU: please give more detail on what is being cited in reference 26.

Q23 APT to AU: please give publisher and publisher location of conference proceedings cited in reference 28.

Q24 APT to AU: please give more information on what is being cited in reference 63.

Q25 APT to AU: please give full title and publisher location for reference 162.

Q26 APT to AU: Ref. 174 is not cited in text, please add them at appropriate place.

Q27 APT to AU: Please check author name 'We' in the ref. 228.